

AD-A186 822

STUDIES ON NONLINEAR MECHANISMS OF EXCIMER LASER  
PROPAGATION IN FLUIDS. (U) UNIVERSITY OF SOUTHERN  
CALIFORNIA LOS ANGELES CENTER FOR LASER... I CANINE

1/1

UNCLASSIFIED

31 JUL 87 CLS-87-15 AFOSR-IR-87-1372

P/C 5/3

NL

END

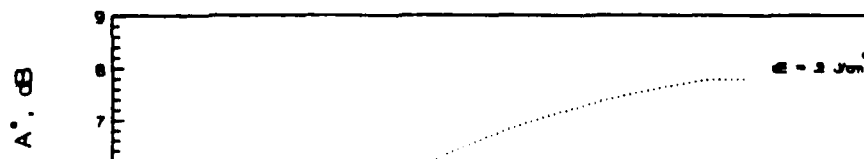
DATE

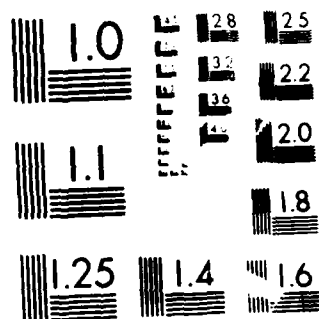
FILED

18

Figure 3.

INDUCED ABSORPTION AT VARIOUS  
IRRADIATION LEVELS





METRIC LINE RESOLUTION TEST CHART  
 NATIONAL BUREAU OF STANDARDS-1963-A

SECURITY CLASSIFICATION OF THIS PAGE

1. REPORT SECURITY CLASSIFICATION <b>UNCLASSIFIED</b>		<b>AD-A186 822</b>		ENTATION PAGE	
2a. SECURITY CLASSIFICATION				1d. RESTRICTIVE MARKINGS	
2b. DECLASSIFICATION/DOWNGRADING SCHEDULE				3. DISTRIBUTION/AVAILABILITY OF REPORT  <b>UNLIMITED</b>	
4. PERFORMING ORGANIZATION REPORT NUMBER(S)  <b>CLS-87-15</b>				5. MONITORING ORGANIZATION REPORT NUMBER(S)  <b>AFOSR-TR- 87-1372</b>	
6a. NAME OF PERFORMING ORGANIZATION  <b>CENTER FOR LASER STUDIES.</b>	6b. OFFICE SYMBOL (If applicable)  <b>CLS</b>	7a. NAME OF MONITORING ORGANIZATION  <b>AFOSR</b>			
6c. ADDRESS (City, State and ZIP Code)  <b>Los Angeles, CA 90089-1112 University of Southern California</b>		7b. ADDRESS (City, State and ZIP Code)  <b>Building 410 Bolling AFB DC 20332-6448</b>			
8a. NAME OF FUNDING/SPONSORING ORGANIZATION  <b>AFOSR</b>	8b. OFFICE SYMBOL (If applicable)  <b>NP</b>	9. PROCUREMENT INSTRUMENT IDENTIFICATION NUMBER  <b>AFOSR-85-0197</b>			
8c. ADDRESS (City, State and ZIP Code)  <b>Bldg 410 Bolling AFB DC 20332-6448</b>		10. SOURCE OF FUNDING NOS.			
		PROGRAM ELEMENT NO. <b>611004</b>	PROJECT NO. <b>2501</b>	TASK NO. <b>A1</b>	WORK UNIT NO.
11. TITLE (Include Security Classification) <b>STUDIES ON NONLINEAR MECHANISMS OF EXCIMER LASER PROPAGATION IN FUSED SILICA FIBERS</b>					
12. PERSONAL AUTHOR(S)  <b>Elsa Garmire</b>					
13a. TYPE OF REPORT  <b>FINAL</b>	13b. TIME COVERED FROM <b>may 1 85</b> TO <b>4/30/87</b>	14. DATE OF REPORT (Yr., Mo., Day) <b>July 31, 1987</b>		15. PAGE COUNT <b>28</b>	
16. SUPPLEMENTARY NOTATION  <b>Prepared in cooperation with Greg Hall and Katherine Liu</b>					
17. COSATI CODES			18. SUBJECT TERMS (Continue on reverse if necessary and identify by block number)		
FIELD	GROUP	SUB. GR.	UV fibers, color centers, excimer lasers, Raman four wave mixing, anti-Stokes, up-conversion		
19. ABSTRACT (Continue on reverse if necessary and identify by block number)  This study was to investigate the potential for short wavelength generation through Raman up-conversion in UV-transmitting fibers. The study resulted in three key achievements:  (continued on the other side)					
20. DISTRIBUTION/AVAILABILITY OF ABSTRACT  <b>UNCLASSIFIED/UNLIMITED</b> <input checked="" type="checkbox"/> SAME AS RPT. <input checked="" type="checkbox"/> DTIC USERS <input checked="" type="checkbox"/>			21. ABSTRACT SECURITY CLASSIFICATION  <b>UNCLASSIFIED</b>		
22a. NAME OF RESPONSIBLE INDIVIDUAL  <b>DR. HOWARD K. SCHWABER</b>			22b. TELEPHONE NUMBER (Include Area Code) <b>(202) 767-4500</b>	22c. OFFICE SYMBOL  <b>NP</b>	

DD FORM 1473, 83 APR

EDITION OF 1 JAN 73 IS OBSOLETE.

SECURITY CLASSIFICATION OF THIS PAGE

1. Identification of induced absorption in fused silica UV fibers due to color center formation with the excimer laser at 193 nm. This is the first time such color center formation has been observed, at several orders of magnitude lower powers than the previously identified "brittle spot formation" optical damage mechanism. A comparison was made of quartz fibers from several vendors and of alternatives, such as liquid core fibers. No better fibers appear available for UV transmission (except perhaps single crystal fibers).

Optical bleaching to reverse the induced absorption was observed by using a longer wavelength of the excimer laser (XeF at 351 nm). A maximum recovery of 70% of initial transmission was obtained. This is the first time that color center formation and subsequent bleaching has been reported in UV-transmitting fibers.

2. Development of new means to image single pulses from the excimer laser, utilizing a phosphor to down-convert the image to the visible, along with a conventional TV camera and videorecorder.

3. Study of Raman up-conversion using excimer lasers. Comparison was made of fibers vs. Raman resonators. Limited coherence length because of the bandwidth spread of excimer lasers and unavailability of low-mode-number UV fibers are reasons why the Raman resonator appears to be a reasonable approach.

Final Report

STUDIES ON NONLINEAR MECHANISMS OF  
EXCIMER LASER PROPAGATION IN FUSED SILICA FIBERS

Elsa Garmire  
Center for Laser Studies  
University of Southern California  
Los Angeles, CA 90089-1112

Submitted to  
Dr. Howard Schlossberg  
Air Force Office of Scientific Research  
Bolling Air Force Base

X

Project Name/	
Availability Codes	
Unannounced	
Special	

A-1

Abstract:

This study was to investigate the potential for short wavelength generation through Raman up-conversion in UV-transmitting fibers. The study resulted in three key achievements:

1. Identification of induced absorption in fused silica UV fibers due to color center formation with the excimer laser at 193 nm. This is the first time such color center formation has been observed, at several orders of magnitude lower powers than the previously identified "brittle spot formation" optical damage mechanism. A comparison was made of quartz fibers from several vendors and of alternatives, such as liquid core fibers. No better fibers appear available for UV transmission (except perhaps single crystal fibers).

Optical bleaching to reverse the induced absorption was observed by using a longer wavelength of the excimer laser (XeF at 351 nm). A maximum recovery of 70% of initial transmission was obtained. This is the first time that color center formation and subsequent bleaching has been reported in UV-transmitting fibers.

2. Development of new means to image single pulses from the excimer laser, utilizing a phosphor to down-convert the image to the visible, along with a conventional TV camera and videorecorder.

3. Study of Raman up-conversion using excimer lasers. Comparison was made of fibers vs. Raman resonators. Limited coherence length because of the bandwidth spread of excimer lasers and unavailability of low-mode-number UV fibers are reasons why the Raman resonator appears to be a reasonable approach.

STUDIES ON NONLINEAR MECHANISMS OF  
EXCIMER LASER PROPAGATION IN FUSED SILICA FIBERS

TABLE OF CONTENTS

I. Executive Summary.....	3
II. Color Center Formation and Bleaching in Fibers.....	6
III. Technique for Imaging Single UV Laser Pulse.....	16
IV. Investigation of Liquid Core UV Fibers.....	18
V. Investigations toward Short Wavelength Anti-Stokes Generation by Stimulated Four-Photon Mixing.....	20

STUDIES ON NONLINEAR MECHANISMS OF  
EXCIMER LASER PROPAGATION IN FUSED SILICA FIBERS

I. EXECUTIVE SUMMARY

In the search for short wavelength sources, one possible mechanism is up-conversion using stimulated Raman scattering (SRS). Previous work at the Center for Laser Studies demonstrated the longer wavelength Stokes shift using the excimer laser in UV fibers [Rothschild and Abad, Opt. Lett. 8, 653 (1983)]. These results led to the suggestion of using SRS to cause stimulated four-photon mixing and anti-Stokes frequency up-conversion into even shorter wavelengths. This AFOSR program has been to investigate this possibility.

The results of this study have been four-fold:

1. While Stimulated Raman Scattering produces longer-wavelength Stokes light effectively in fibers, the difficulty of fiber mode-matching as well as the broad band of the excimer laser radiation increases the four-photon mixing threshold to prohibitive levels. The coherence length introduced by this laser bandwidth at 193 nm is less than 50 cm, which means that the fiber cannot provide the km of length which have generated anti-stokes so successfully in the visible. Indeed, because inherent loss in UV fibers also limits useful lengths to less than 50 cm, fibers have no advantage over resonators. For this reason fibers may have a limited potential for frequency up-conversion with excimer lasers, and we decided to explore the potential of Raman resonators.
2. A few liquids, highly transparent in the UV, have been identified which may be incorporated in an external Raman Resonator in order to create strong Stokes Raman light. This Stokes light, resonated at the appropriate small phase-matching angle, will generate anti-Stokes using four-photon mixing with the UV excimer laser. Design calculations show that short-wavelength generation by four-photon mixing is possible using the 193 nm excimer laser. Design calculations include quartz as well as the low-loss liquids, water and acetonitrile. This is the method we are currently proposing for Raman wavelength up-conversion. We identified acetonitrile and water from extensive measurements of the UV transmission of liquids. Our original motivation was to search for the possibility of a liquid core fiber. Unfortunately all low-loss liquids have refractive index less than fused silica, so that we have not been able to identify UV-transmitting liquid core fibers.



3. At fluence levels which might be expected to cause nonlinear effects in fused silica fibers, we have observed that color center formation degrades transmission after multiple shots. We have also shown that subsequent bleaching with irradiation at longer wavelengths is possible. The results will be submitted for publication in Applied Physics Letters and presented at the Optical Society Annual Meeting.

4. In the pursuit of our experimental research it was necessary to develop a means to measure two-dimensional images of single 10 nsec pulsed excimer laser output far field patterns. The only existent technology was very expensive UV video tubes, two dimensional CCD arrays or very slow photography. We developed a technique which used a phosphor to down-convert the image to the visible which was then recorded by a conventional TV camera and video-recorder. Successive TV scans measured various levels of decreasing fluorescence over a millisecond period. This allowed high resolution images to be measured over at least four orders of magnitude in dynamic range. The results were presented at CLEO and published in Applied Optics.

The research supported under this two-year program has led to three papers and a Master's thesis. The first paper was the single-pulse imaging system, published in Applied Optics. It is attached as Section III of this report. The other two papers are under preparation at the present time and describe the color center formation and bleaching. Section II is a compilation of these results. This is the MS thesis work of Greg Hall.

Three talks have or will be presented covering work funded on this AFOSR program. These are at CLEO, OSA annual meeting and LEOS, Southern California Chapter. Table I outlines these presentations and lists the personnel whose research was partially funded by this program.

Section IV contains a short review of our investigation of liquids for possible use in liquid core UV fibers. This work identified water and acetonitrile as low loss UV transmitting liquids. Section V contains the theoretical modelling for Stimulated Four-Photon Mixing in fibers and Raman resonators and represents the basis on which we make recommendations to discontinue research on upconversion in fibers and to concentrate Raman resonators.

Table I. Funded Personnel and Reports of Research

Personnel

Elsa Garmire, Principal Investigator  
Katherine Liu, PhD Student: PhD still in progress  
Greg Hall, MS student: MS granted, August, 1987

Theses Completed

MS Thesis entitled: "Studies of Color Center Formation and Bleaching in UV Fibers using Excimer Lasers" by Greg Hall

Papers

1. K. Liu, M. Neudorffer, E. Garmire, "Technique for imaging single UV laser pulses" Applied Optics, 25, 2472, 1986.
2. G. Hall and E. Garmire, "Color Center Formation and Bleaching by Excimer Lasers in UV Fibers", to be submitted to Applied Physics Letters
3. G. Hall and E. Garmire, "Studies of UV Laser Transmission in Fused Silica Fibers" to be submitted to Applied Optics

Presentations

1. K. Liu, M. Neudorffer, E. Garmire, "Technique for imaging single UV laser pulses", CLEO, 1986
2. K. Liu, M. Neudorffer, E. Garmire, "Technique for imaging single UV laser pulses", LEOS, Southern California Chapter, October, 1985
3. G. Hall and E. Garmire, "Color center formation and bleaching in UV-transmitting fibers", Opt. Soc. of Am. Annual Meeting, 1987

## II. COLOR CENTER FORMATION AND BLEACHING IN UV FIBERS

Greg Hall and Elsa Garmire

### A. Introduction

In experiments on nonlinear effects in fused silica fibers using ArF excimer lasers with wavelength of 193 nm, we observed a transmission decay with time and identified this as due to color center formation. This color center formation occurs at fluence levels as much as two orders of magnitude lower than those required for catastrophic degradation ("brittle spot" formation [1]). Color center formation occurs when the fused silica fibers are irradiated with an ArF laser (wavelength = 193 nm) at fluences ranging from 6 to 200 mJ/cm<sup>2</sup> per pulse.

The proof that these are color centers is obtained by bleaching them. As a consequence of the meta-stable nature of color centers, the induced absorption is reversible via bleaching schemes [2]. We report for the first time the optical bleaching of UV absorption bands resulting from UV irradiation damage in fused silica fibers. This complements previous investigations [3-5] in which high energy gamma rays produced bleachable absorption bands in the visible to IR spectrum.

In addition to these bleaching experiments, studies of color center growth kinetics show that the data correlates with a simple mathematical model. Two parameters, the absorption saturation limit and the damage rate constant, characterize the fiber performance. The dependence of these parameters on input fluence, fiber length and manufacturer is documented.

### B. Experimental Procedure

The apparatus used to obtain induced absorption data was set up to measure single-pulse transmission with variable input fluence. Evidence of induced optical damage appeared as a relative transmission drop during irradiation intervals.

The UV radiation source was a Lumonics K-261 multi-gas excimer laser in the stable resonator configuration. Two different gas mixtures were utilized: ArF, providing the damaging radiation at a wavelength of 193 nm; and XeF, providing the bleaching light at 351 nm. When operating with ArF, the laser produced 10 ns pulses at peak powers of > 1.4 MW. Coupling of the output beam to the fiber was accomplished by three plano-convex quartz lenses. Two silicon photo-diode detectors were employed. One, acting as a reference detector, was located between the variable input attenuator and the fiber input tip and monitored the input fluence. The second, acting as the signal detector, monitored the

fluence emerging from the fiber. When calibrated, the ratio of the detectors yielded the transmission information. Signals from the detectors were fed into a two-channel oscilloscope and recorded via video equipment.

Samples from three different manufacturers were tested. All were step-index, high OH-content, glass clad fibers with 200  $\mu\text{m}$  fused silica cores. The fibers with the best transmission, and hence the ones used predominantly, were the SG-840 series provided by SpecTran Corp. The cladding of these fibers was fluorine-doped. Other fibers studied were the EOTec 301002 and Diaguide ST-U200D-SY series, both with BR-doped claddings. Since fused silica is very lossy at 192 nm (a 50 cm segment of SpecTran fiber has a typical transmission of 20%), only short fiber samples from 25 to 100 cm long were used. All absorption measurements were taken on straight fibers, held in position by inserting into thin glass capillaries. Surface quality of the tip was maintained smooth and flat without polishing; the result of a clean fracture when cleaving. Irradiation intervals were conducted at a rep rate of 1 pps, and continued until the fiber's transmission dropped to a terminal value. Spontaneous recovery tests were performed on several samples with the result of no improvement in transmission when left undisturbed for two hours in room lighting.

### C. Theory

Photons at 193 nm have sufficient energy to interact with the valence band of oxygen atoms, producing excitons, whose holes can be trapped at potential wells associated with lattice defects. When this trapping occurs, a color center is born. An absorption band develops because the hole can either assume an excited state or become completely ionized when interacting with incoming photons. The ionization of a trapped hole is known as bleaching. If the bleaching photon energy is below the exciton production threshold, but has sufficient energy to ionize the trapped holes, color center levels will drop and the fiber will experience at least a partial recovery of its transmission.

Mathematically, induced absorption and color center growth are proportional [2]. For the studies reported here we will use the following form:

$$A = A_s [1 - \exp(-E/E_0)],$$

where  $A$  is the induced absorption (in dB),  $A_s$  is the absorption saturation limit,  $E$  is the total fluence of damaging radiation, and  $E_0$  is the damage rate constant. This expression assumes only one mechanism for color center formation and the absence of optically caused lattice defects. At higher fluences such lattice

defects can be created, leading to "brittle spot" formation [1].

When color centers already exist at the beginning of the irradiation interval, the above equation is modified slightly to

$$A = A_s [1 - C \exp(-E/E_0)],$$

where  $C = 1 - N_0/N_s$ ;  $N_0$  is the pre-existing color center population and  $N_s$  is the color center saturation limit proportional to the induced absorption saturation limit. This equation is useful in the analysis of bleaching experiments.

#### D. Results

##### 1. Induced Absorption

When the first pulse of light is launched into a fiber, the initial transmission,  $T_0$ , is established. It was found that  $T_0$  varied substantially from one fiber to the next. For example, several 50 cm SpecTran fibers were irradiated at a fluence of 0.02 J/cm<sup>2</sup> per pulse. The average  $T_0$  was 20%, but varied from 2% to 40%, depending on sample. In spite of the disparity, all of these fibers developed approximately the same fraction of induced absorption. Typically the transmission dropped to a terminal value of approximately 33% of the original transmission. A typical value is shown in Figure 1. No spontaneous recovery of transmission was observed.

##### 2. Optical Bleaching

Figure 2 shows the data and theoretical curves for a representative fiber during a bleaching experiment. In this instance, a 50 cm long SpecTran fiber was irradiated at a fluence of 20 mJ/cm<sup>2</sup> per pulse. During the pre-bleach interval a new fiber sample was exposed to ArF radiation, causing induced absorption from color center formation. Saturation eventually occurs because of the finite number of pre-existing lattice defects at which color centers can form. The bleaching interval is represented by the vertical dashed line, wherein a total fluence of approximately 13 J/cm<sup>2</sup> at 351 nm was delivered to the fiber. Evidence of successful bleaching is provided in the post-bleach interval by re-irradiating the fiber at 193 nm and noticing that the induced absorption has fallen from its saturation value of 3.46 dB to 1.54 dB, a 55% reduction equivalent to a transmission recovery of 70%. Again, the induced absorption follows a curve similar to the pre-bleach interval, saturating at the same value.

##### 3. Induced Absorption at Varied Irradiation Levels

For these studies all experimental parameters were held constant, except for the input fluence per pulse: 50 cm lengths of SpecTran

Figure 1.

# INDUCED ABSORPTION VS. TOTAL FLUENCE

$$A^* = 5.50(1 - e^{-E/3.82})$$

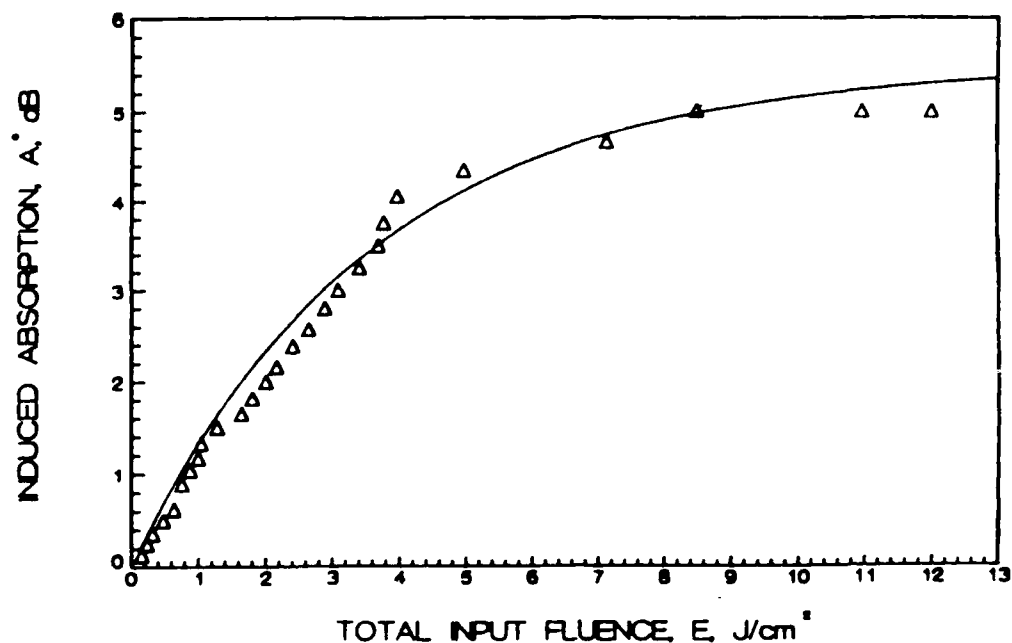
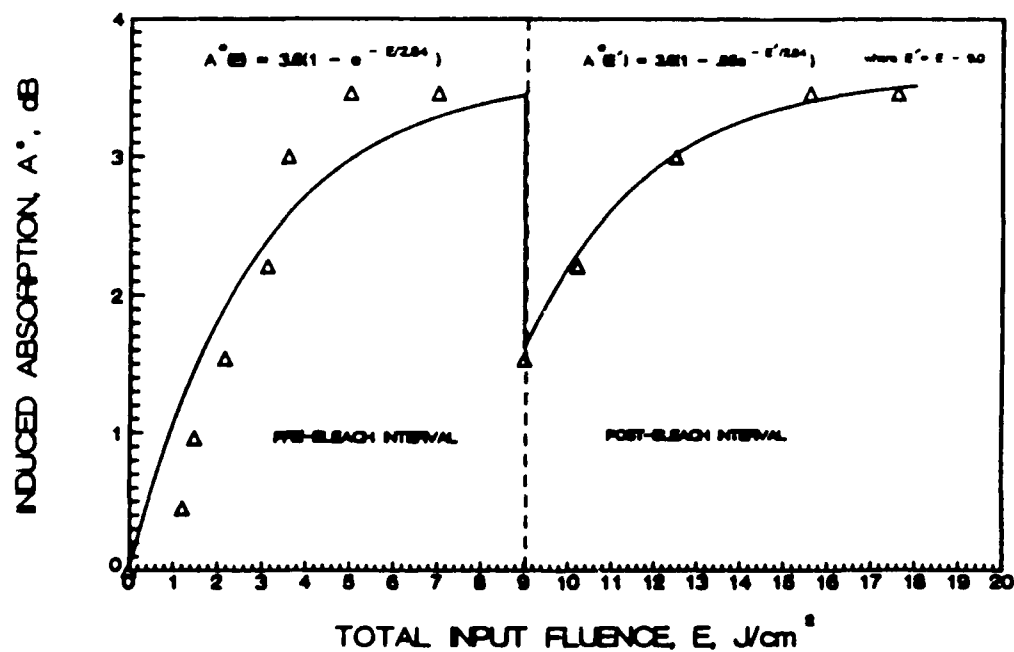


Figure 2. INDUCED ABSORPTION BEFORE AND AFTER OPTICAL BLEACHING



fiber were used. At each fluence level at least two fibers were tested. By averaging the measurements,  $A_s$  and  $E_0$  were determined and a set of design curves was generated as a way of averaging the data. The results are shown in Figure 3. No induced absorption was seen at the  $2 \text{ mJ/cm}^2$  level, implying the existence of a color center formation threshold somewhere between 2 and  $6 \text{ mJ/cm}^2$ . At  $200 \text{ mJ/cm}^2$  and above, occasional catastrophic damage occurred where the transmission suddenly dropped to zero, presumably due to brittle spot damage as identified by Nevis [1]. When operating at  $20 \text{ mJ/cm}^2$  and below, brittle spot damage never appeared. Apparently the  $200 \text{ mJ/cm}^2$  fluence level was near the brittle spot threshold.

From our results it can be seen that the absorption saturation limit,  $A_s$ , increases with input fluence per pulse. Table II.1. shows the induced absorption parameters at different fluences which were determined by fitting experimental data. Studies are underway to understand the reason for the increase in both  $A_s$  and  $E_0$  with increasing fluence per pulse.

#### 4. Induced Absorption at Varied Lengths

SpecTran fiber samples were tested with fluence level held constant at  $20 \text{ mJ/cm}^2$  per pulse and the length varied. The induced absorption parameters determined from these measurements are shown in Table II.2.

#### 5. Induced Absorption of Selected Commercial Fibers

In addition to SpecTran fibers, both EOTec and Diaguide fibers were tested. The results are shown in Table II.3. The fibers were cut to 50 cm lengths and irradiated at a fluence level of  $20 \text{ mJ/cm}^2$  per pulse. At least two fibers of each brand were tested. The parameters were determined by averaging the measurements and were used to produce the design curves shown in Figure 4. Also of interest is the fact that the average initial transmission of both SpecTran and EOTec fibers was 20%, whereas Diaguide fibers had a value of only 2%.

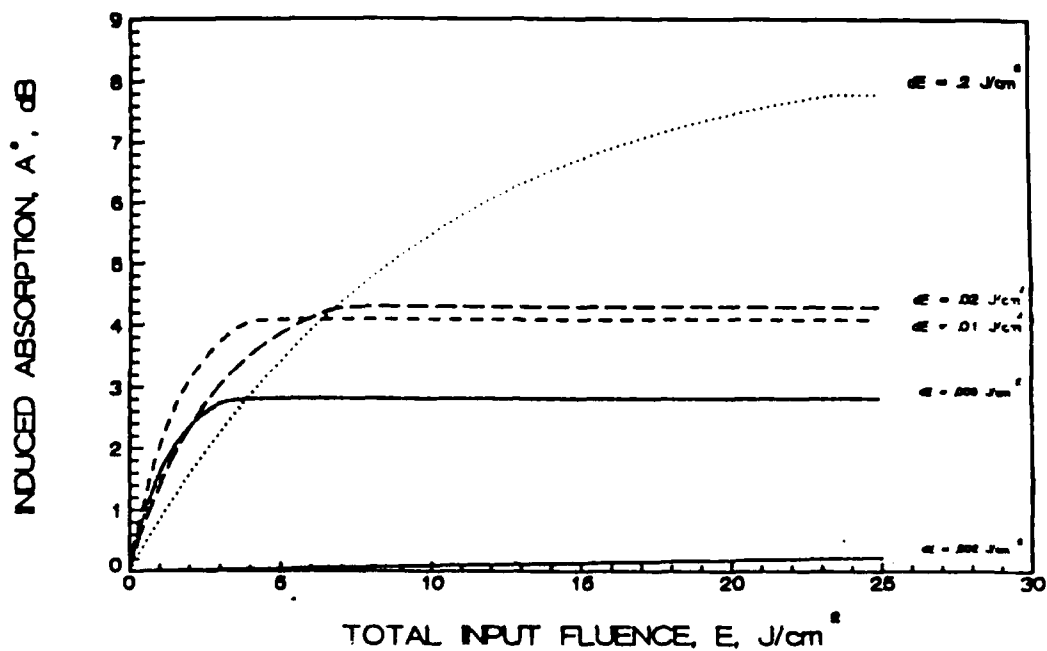
It is clear that the best performer is the SpecTran fiber, as its damage level is more than two times less than the others. The main difference between the different fibers is the type of cladding. SpecTran fibers are P-doped whereas the other two are BF-doped.

#### E. Conclusion

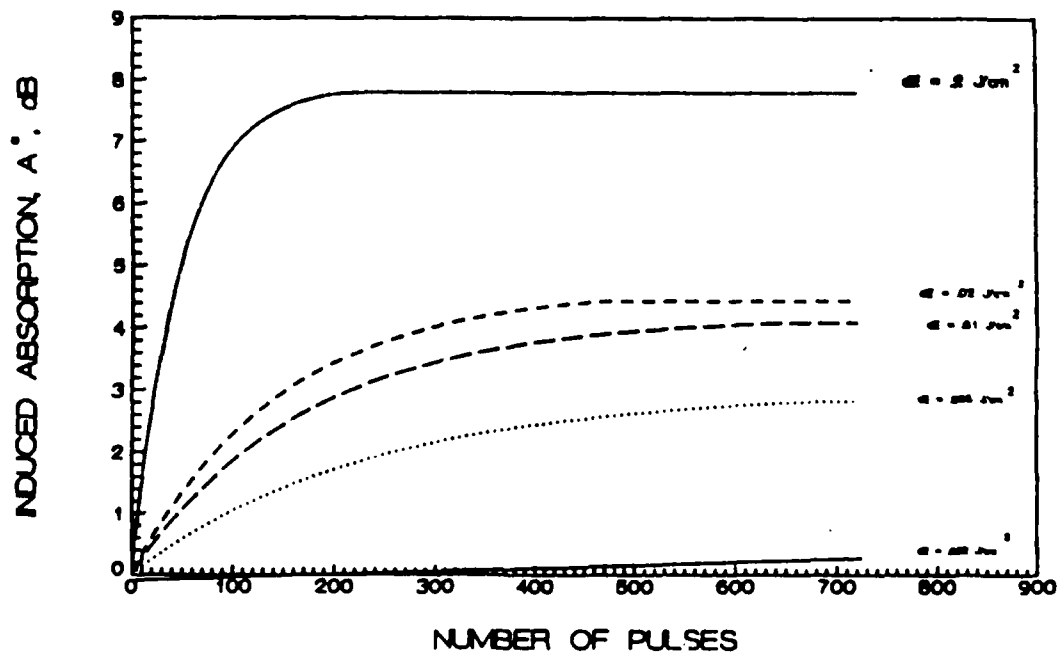
Evidence has been presented which identifies a class of ultra-violet damage attributed to the presence of color centers in fused silica fibers. Although an exhaustive study was not performed it is believed that the same phenomenon exists at other

Figure 3.

# INDUCED ABSORPTION AT VARIOUS IRRADIATION LEVELS



# INDUCED ABSORPTION AT VARIOUS IRRADIATION LEVELS





# TABLE 1

INDUCED ABSORPTION PARAMETERS AT DIFFERENT FLUENCES

$dE$ ( $J/cm^2$ )	$A_e$ (measured) ( dB )	$E_o$ ( J )
.002	0	—
.006	2.82	1.41
.01	4.10	1.72
.02	4.31	2.96
.2	7.78	9.81

**TABLE 2****INDUCED ABSORPTION AT VARIOUS FIBER LENGTHS**

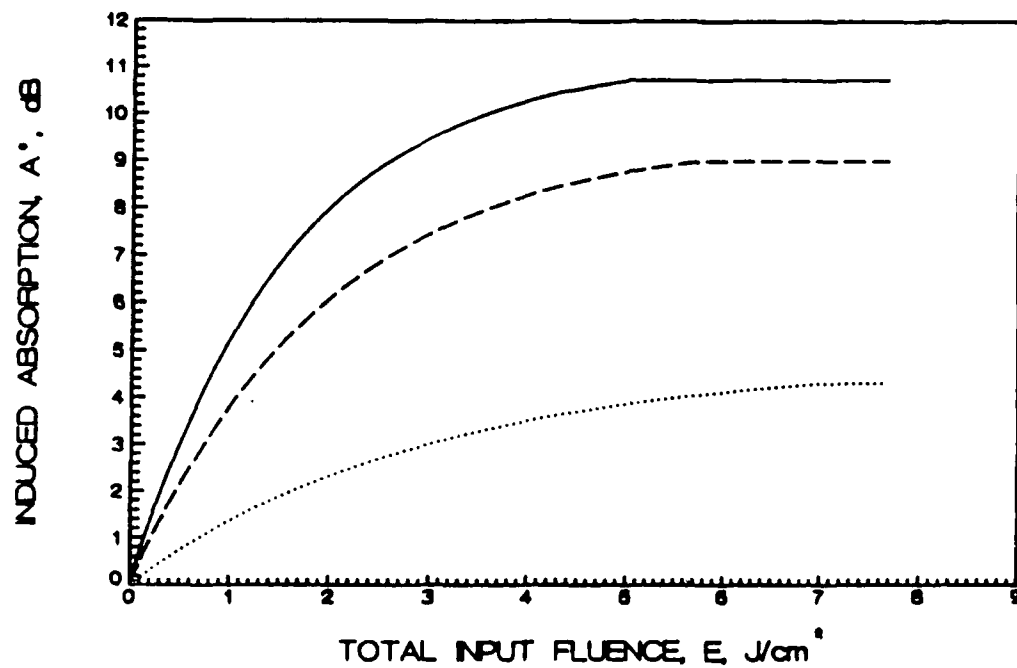
<b>LENGTH ( cm )</b>	<b>A . ( dB )</b>	<b>E . ( J )</b>
<b>25</b>	<b>3.73</b>	<b>5.07</b>
<b>50</b>	<b>4.31</b>	<b>2.96</b>
<b>100</b>	<b>6.22</b>	<b>5.98</b>

**TABLE 3****INDUCED ABSORPTION PARAMETERS OF SELECTED FIBERS**

<b>MANUF. CTURER</b>	<b>FIBER TYPE</b>	<b>AVERAGE INTAL TRANSMISSION</b>	<b>A . dB</b>	<b>E . J</b>
<b>SpecTran SG - 840</b>	<b>High OH- fused silica F - doped cladding</b>	<b>20 %</b>	<b>4.31</b>	<b>2.96</b>
<b>EOTec PIN 301002</b>	<b>High OH- fused silica BF - doped cladding</b>	<b>20 %</b>	<b>8.98</b>	<b>1.95</b>
<b>DIAGUDE ST - 10000 - 87</b>	<b>High OH- fused silica BF - doped cladding</b>	<b>2 %</b>	<b>10.7</b>	<b>1.59</b>

# INDUCED ABSORPTION OF SELECTED COMMERCIAL FIBERS

— DIAGUDE      - - - EOTec      ..... SpecTran



UV wavelengths, such as the KrF line at 248 nm. Color center growth and bleaching studies at this wavelength would be interesting, since Nevis has noticed a strong propensity towards induced brittle spot damage in fibers irradiated at 248 nm. It is also probable that a bleaching wavelength other than 351 nm (perhaps XeCl at 308 nm) would have a higher recovery efficiency.

#### P. References

1. E. A. Nevis, "Alteration of the Transmission Characteristics of Fused Silica Optical Fibers by Pulsed Ultraviolet Radiation", SPIE, 540, 421-426 (1985).
2. J. H. Schulman, W. D. Compton Color Centers in Solids The MacMillan Company, New York, 1962
3. R. H. West, A. P. Lenham, "Characteristics of Light Induced Annealing in Irradiated Optical Fibers", Electr. Lett. 18, 483 (1982).
4. E. J. Friebele, M. E. Gingerich, "Photo-bleaching Effects in Optical Fiber Waveguides" Applied Optics, 20, 3448-3452 (1981)
5. E. M. Dianov, L. S. Kornienko, E. P. Nikitin, A. O. Rybaltovskii and P. V. Chernov, "Reversible Optical Bleaching of the Induced Absorption in Fiber-Optics Waveguides" Sov. J. Quan. Electr. 9, 636-637. (1979)

### III. Technique for imaging single UV laser pulses

Katherine X. Liu, Mary Neudorffer, and Elsa Gamire

University of Southern California, Center for Laser Studies, Los Angeles, California 90089-1112.

Received 22 April 1986.

0003-6935/86/152472-02\$02.00/0.

© 1986 Optical Society of America.

Pulsed UV sources, such as excimer lasers, provide difficult requirements for an imaging system. Pulse intensity and spatial profile variations from shot to shot require a large dynamic range and high resolution in an imaging detector. We have developed an inexpensive fluorescent imaging system which uses the concept of an ordinary video camera and video cassette recorder to record the decay of fluorescence with time. The successive images on the VCR decrease in intensity as the fluorescence decays, allowing the operator to choose the optimum exposure. This provides over 1000 dynamic range with a spatial resolution measured to be better than  $25\ \mu\text{m}$ . This performance is comparable to commercially available CCD arrays.

The use of fluorescent material to convert UV to visible for UV imaging is common practice with the visible image typically recorded with a CCD array.<sup>1-5</sup> The technique we developed offers a permanent record of images in real time which is of considerable usefulness in medical and other applications of UV pulsed lasers. The UV image was converted to a visible image by impinging on a semitransparent fluorescent screen. A video camera focused to the back of the fluorescent screen provided real-time images. However, variability in power from shot to shot and the relatively low dynamic range of a video camera made proper exposure very difficult. Therefore, a VCR was used to record the beam image of each pulse via a series of scan frames. The decay of visible emission from the fluorescent material provided a graduated set of exposures for successive scan frames on the videotape. These frames could be played back immediately and stopped on the frame with the proper exposure so that the beam profile characteristics could be assessed in near real time. Polaroid photographs of the videotape displays were made when hard copies were needed.

The laser source used in our experiments was a 320-nm beam from a doubled dye laser with an  $\sim 1\text{-cm}$  diameter and energy of  $\sim 10\text{--}20\text{ mJ}$  in a pulse of 300-ns length. A glass plate was spin-coated with a thin layer of fluorescent paint

(DAYGLO pigments<sup>6</sup>) so that a visible image appeared in fluorescence on the back side of the screen. Our experiments were performed with a signal green and blaze orange pigments. Based on the emission data for these pigments, the signal green pigments provided the best match to the video camera response curve, but the blaze orange has a higher luminance, as shown in Fig. 1.<sup>6,7</sup> The data shown here was taken with blaze orange. We have not made a careful comparison of two in identical circumstances.

The decay time of the fluorescent paint was sufficiently long to allow recording of many frames of different exposures on the videotape for each pulse. The decay time (to  $1/e$ ) is  $\sim 55\text{ ms}$ . The frame rate is 18.6 ms. Typical data are shown in Fig. 2. The videotape could then be replayed by advancing the tape a single frame at a time, and the best exposure could be selected.

The spatial resolution of the system was found to be better than  $25\ \mu\text{m}$ , as demonstrated in Fig. 3, which shows a Polaroid photograph of a video frame taken with 25-, 80-, and 125- $\mu\text{m}$  wires placed in the laser beam next to the fluorescent film.

The dynamic range for the camera and fluorescent paint combination, i.e., for a single frame, was limited by the video camera and estimated to be of the order of 10. However, the simultaneous multiple exposures obtained in successive scan frames with the VCR were  $>100$ . Together with the single-frame range of 10, this provides an effective dynamic range of

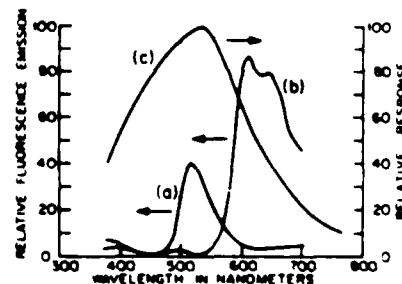


Fig. 1. (a) Emission spectra for DAYGLO signal green pigment.<sup>6</sup> (b) Emission spectra for DAYGLO blaze orange pigment.<sup>6</sup> (c) Spectral response characteristic for RCA TC1000 video camera.<sup>7</sup>



Fig. 2. Representative scan frames from single pulse showing multiple exposure settings that can be obtained with this technique.



Fig. 3. Image of wire grid used to determine detector resolution. The far right pair of lines are 25- $\mu\text{m}$  gold wires. The center pair are 80- $\mu\text{m}$  hairs. The far left three wires are 185- $\mu\text{m}$  transformer wires.

>1000. This aspect of the system can be seen in Fig. 2, which shows how structure can be resolvable in one frame that is not clear in another. The ultimate limit to the dynamic range is given by halation of the video camera.

The linearity of the fluorescent screen was verified by comparison with a power meter for incident pulse intensities from  $\sim 3$  to  $\sim 16 \text{ kW/cm}^2$ . The maximum power is limited by damage to the fluorescent paint, which we observed at  $1 \text{ MW/cm}^2$ . The total number of bits is determined by the TV

system at  $\sim 1.6 \times 10^5$ , and the image area can easily be as large as  $8 \times 10 \text{ cm}$ .

The 25- $\mu\text{m}$  resolution and 1000 effective dynamic range compare favorably to the best CCD arrays. But the imaging area may be much bigger than that of CCDs. For example, the Ford Aerospace and Communications Corp.  $1024 \times 1024$  visible imager has a resolution of  $17 \mu\text{m}$  and dynamic range of 60 dBV (i.e.,  $10^3$ ), but this CCD array has only  $\sim 2 \times 2\text{-cm}$  imaging area.

The work was funded in part by AFOSR.

#### References

1. C. I. Coleman, "Image Detectors for the Ultraviolet," *Appl. Opt.* **20**, 3693 (1980).
2. N. Kristianpoller and D. Dutton, "Optical Properties of Liomogen: a Phosphor for Wavelength Conversion," *Appl. Opt.* **3**, 287 (1964).
3. W. M. Burton and B. A. Powell, "Fluorescence of Tetraphenylbutadiene in the Vacuum Ultraviolet," *Appl. Opt.* **12**, 87 (1973).
4. M. W. Cowens, M. M. Blouke, T. Fairchild, and J. A. Westphal, "Coronene and Liomogen as VUV Sensitive Coatings for Si CCD Imagers: a Comparison," *Appl. Opt.* **19**, 3727 (1980).
5. H. O. Pritchard, R. W. Nicholls, and A. Lakshmi, "Ultraviolet Sensitization of Silicon Detectors for Space Astronomical Applications," *Appl. Opt.* **18**, 2085 (1979).
6. Day-Glo Technical Bulletin 2002. DAYGLO is a registered trademark of Day-Glo Color Corp.
7. RCA TC1000 literature.

#### IV. INVESTIGATION OF LIQUID CORE UV FIBERS

Katherine X. Liu and Elsa Garmire

Organic liquids have been preliminarily investigated for possible use as a core material of UV-transmitting liquid fibers for nonlinear interactions. We have found that some liquids are usable for wavelengths of 249 nm and above from excimer lasers, but none of them is suitable for 193 nm.

Organic liquids for possible candidates of UV liquid core fibers have been examined with the help of chemists at USC. Table 1 lists a large number of liquids whose refractive indices are larger than quartz at wavelength of 589.3nm (1.4584) [1]. We chose a few liquids identified as the most likely for high UV transmission, such as cyclohexanol, dimethylsulfoxide (DMSO), 1,2,3-propanetriol (Glycol), decahydronaphthalene (Decalin), and measured their UV transmission curves. Figure 1 shows the result of the measurements. Cyclohexanol was predicted to be the most transparent in the UV according to the chemists' recommendations using their knowledge of structure theory. The relatively large UV loss may be because the sample was not purified sufficiently. It appears that none of these liquids will be transparent at 193 nm. Cyclohexanol and Glycol have 30% loss/cm at 249 nm (KrF). DMSO has 20% loss/cm at 308 nm (XeCl), and Decalin is usable at 350 nm (XeF).

Of those whose refractive indices are smaller than quartz, acetonitrile was considered a good candidate. The UV transmission measurement shows that the cutoff is almost 193 nm. In addition, water has good UV transmission. These are all shown in Fig. 1. However, the problem is that their refractive indices are lower than quartz, and in order to have fibers we would have to look for some other kind of material with lower refractive index to use as the cladding to make a waveguide.

At this stage, organic liquids are not considered as a suitable way to make UV liquid core fibers to observe stimulated four-photon mixing (SPPM) for obtaining shorter wavelengths. However, because of their high nonlinear susceptibility, it might be possible to use either cyclohexanol or glycol as fiber cores at 249 nm to achieve stimulated Raman effect for obtaining frequency tuning. In addition, straight capillaries of low index liquids may have suitable transmission.

#### Reference

1. Index data for organic compounds from, CRC Handbook of Chemistry and Physics. Florida: CRC Press Inc., 1986. E-370.

# INDEX OF REFRACTION OF ORGANIC COMPOUNDS

		Compound	$n_D$
4-n-Propyl-5-ethylidioxane	1.435	N- $\beta$ -Oxypropyl morpholine	1.462
1,2-Dichloro-2-methylpropane	1.435	2-( $\beta$ -Ethyl)-hexylcyclohexanone	1.463
1,2-Propyleneglycol sulfite	1.435	2-Ethylcyclohexan-1-ol	1.463
N-Methylmorpholine	1.436	Fluorobenzene	1.463
1-Chloro-2-methyl-2-propanol	1.436	d- $\alpha$ -Pinene	1.464
Epichlorohydrin	1.436	l- $\alpha$ -Pinene	1.465
Triethyleneglycol-mono-butyl ether	1.437	Cyclohexanol	1.465
4-Ethyl-7,7,7-trimethyl-1-heptanol	1.438	m-Fluorotoluene	1.465
1-Methyl-3-ethyloctan-1-ol	1.438	p-Fluorotoluene	1.467
1-Ethyl-3-ethylhexan-1-ol	1.438	trans-Decahydronaphthalene	1.468
Diethyl maleate	1.438	o-Fluorotoluene	1.468
1-Butanethiol	1.440	3-Alloxy-2-oxypropylamine-1	1.469
2-Chloroethanal	1.440	Ethanol-1-methylisopropanol amine	1.470
Dibutyl sebacate	1.440	d-Limonene	1.471
1-Ethyl-3-ethyloctan-1-ol	1.441	1,2,3-Trichloroisobutane	1.473
Dimethylmaleate	1.441	Decahydronaphthalene	1.474
3-Methylpentane-2,4-diol	1.441	1,2,3-Propanetriol	1.474
Ethyl sulfide	1.442	Trichloroethylene	1.475
Mesityl oxide	1.442	N- $\beta$ -Oxyethylmorpholine	1.476
Butyl stearate	1.442	Dimethylsulfoxide	1.476
1,2-Dichloroethane	1.444	cis-Decahydronaphthalene	1.479
Chloroform	1.444	N- $\beta$ -Chlorallylmorpholine	1.481
trans-1,2-Dichloroethylene	1.444	n-Dodecyl-4-tertiarybutylphenyl ether	1.482
Diethyleneglycol	1.445	n-Dodecylphenyl ether	1.482
cis-1,2-Dichloroethylene	1.445	n-Dodecyl-4-methylphenyl ether	1.483
3-( $\alpha$ -Butyloctyl)-oxypropyl-1-amine	1.446	2-Ethylidene cyclohexanone	1.486
2-Methylmorpholine	1.446	n-Butylbenzene	1.487
Dipropyleneglycol-monoethyl ether	1.446	p-Cymene	1.488
Formamide	1.446	iso-Propylbenzene	1.489
3-Lauryloxypropyl-1-amine	1.447	Furfuralcohol	1.489
Cyclohexanone	1.448	tert-Butylcumene	1.490
1-Aminopropan-1-ol	1.448	n-Propylbenzene	1.490
Diethyleneglycol-mono- $\beta$ -oxypropyl ether	1.448	sec-Butylbenzene	1.490
1-Amino-2-methylpentan-1-ol	1.449	tert-Butylbenzene	1.490
Tetrahydrofurfural alcohol	1.450	Dibutylphthalate	1.490
2-Propylcyclohexa-1-one	1.452	tert-Butyltoluene	1.491
2-Aminoethanol	1.452	1-Penyl-1-oxyphenylethane	1.491
2-Butylcyclohexan-1-one	1.453	n-Hexylcumene	1.492
Ethylenediamine	1.454	n-Octyltoluene	1.492
2-( $\beta$ -Methyl)-propylcyclohexan-1-one	1.454	n-Octylcumene	1.492
4-Methylcyclohexanol	1.454	p-Xylene	1.493
3-Methylcyclohexanol	1.455	1,31-Diethylbenzene	1.493
bis-2-Chloroethyl ether	1.455	Ethylbenzene	1.493
Cyclohexylamine	1.456	1,3-Dimorpholylpropan-2-ol	1.493
1,8-Cineol	1.456	1,12,2-Tetrachloroethane	1.493
2,2'-Dimethyl-2,2'-dipropyldiethanol amine	1.456	Toluene	1.494
1,1',2,2'-Tetramethyldiethanol amine	1.459	Benzylethyl ether	1.494
1-Aminopropan-3-ol	1.459	m-Xylene	1.495
Carbon tetrachloride	1.459	1,4-Diethylbenzene	1.496
3-Methyl-5-ethylheptan-2,4-diol	1.459	2,3-Dichlorodioxane	1.496
2-( $\beta$ -Ethyl)-butylcyclohexan-1-one	1.461	Mesitylene	1.497
2-Methylcyclohexanol	1.461	2-Iodopropane	1.497
N-(n-Butyl)-diethanol amine	1.461	Benzene	1.498
4,5-Chloro-1,3-dioxolane-2	1.461		
2-Butylcyclohexan-1-ol	1.462		



TRANSMISSION (%) through 1 cm path length

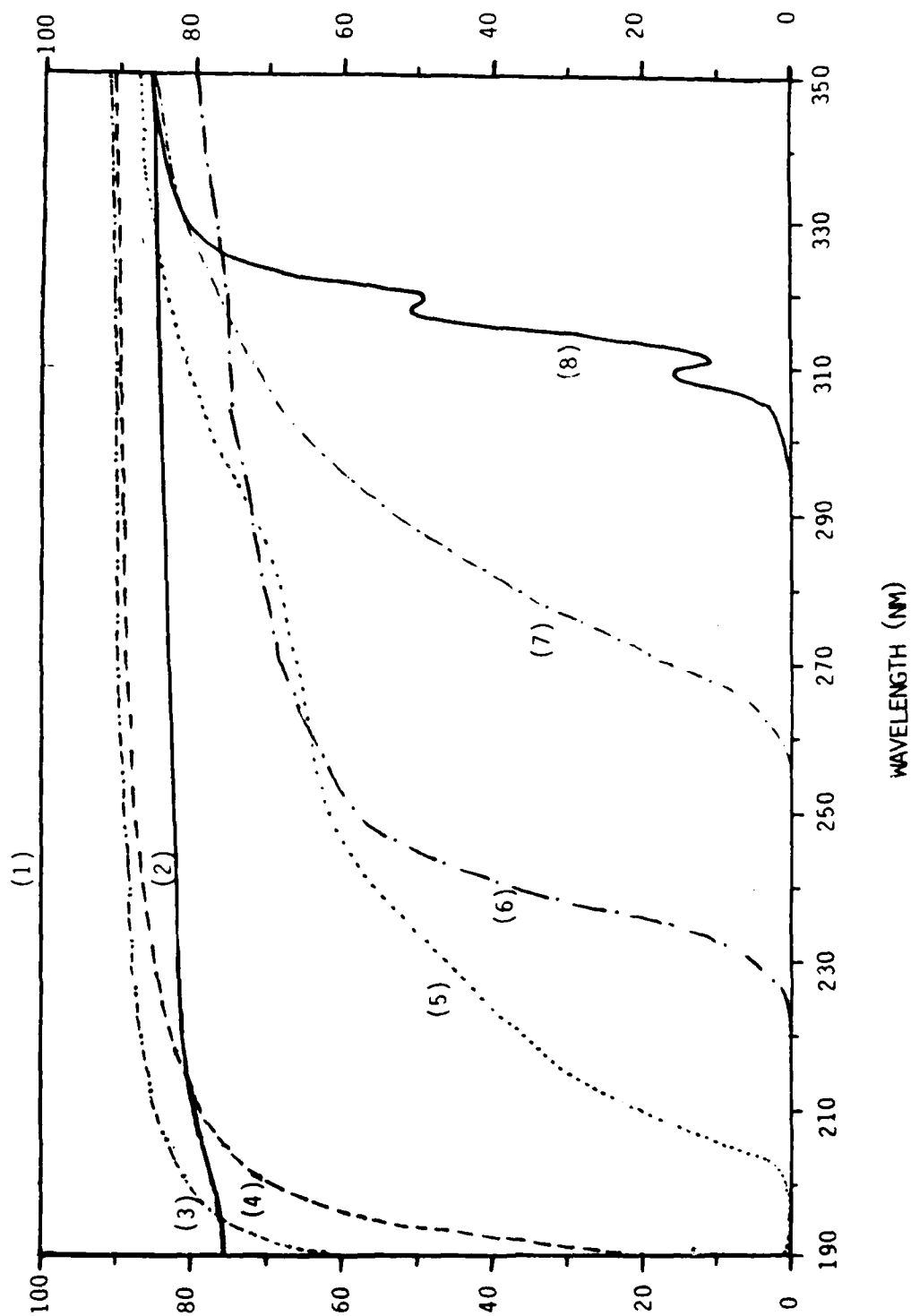


Fig. 1 (1) Air; (2) Quartz cell; (3) H<sub>2</sub>O; (4) Acetonitrile; (5) Glycol  
(6) Cyclohexanol; (7) DMSO; (8) Decalin.

V.

# INVESTIGATIONS TOWARD SHORT WAVELENGTH ANTI-STOKES GENERATION BY STIMULATED FOUR-PHOTON MIXING Katherine X. Liu and Elsa Garmire

## Abstract

The possibility of stimulated four-photon mixing (SFPM) with pump wavelength of UV in fused silica optical fibers has been investigated theoretically. Phase matching by utilizing fiber modes and fiber birefringence are both obtainable. However, efficient four-photon interactions will be limited by the availability of single-mode and low-number-mode UV fibers. Furthermore, the short coherence length of excimer lasers may be a problem for obtaining enough gain to observe large anti-Stokes shifts. The alternative technology of a Raman resonator appears to be a favorable technique for generating short wavelengths.

## 1. Introduction

Four photon mixing is a nonlinear effect associated with the term  $\chi^{(3)}E$  in the polarization expansion (and is also called three wave mixing). It is a process of parametric interactions of four photons (or three waves) with two photons from the pump wave, one photon from the Stokes wave and one photon from the anti-Stokes wave. Under the assumption of no pump depletion and significant Stokes amplification, Maxwell's Equation for anti-Stokes wave (neglecting the intensity dependent phase modulation) becomes [1]

$$i\frac{\partial}{\partial z} E_a(\lambda_a) = -2\mu_0(\pi c/\lambda_a)^2 \text{Re}[\chi^{(3)}] E_p^2(\lambda_p) E_s^*(\lambda_s) e^{-i\Delta k z} \quad (1)$$

where  $\Delta k = k_a + k_s - 2k_p$ ,  $k$  is the wavevector and the subscripts a, s and p denote anti-Stokes, Stokes and pump. The intensity in anti-Stokes is therefore given by integration of Eq. (1) and has the form

$$I_a = \left(\frac{\mu_0}{\epsilon_0}\right)^2 \frac{(2\pi c/\lambda_a)^2}{n} (\text{Re}[\chi^{(3)}])^2 I_p^2 I_s L^2 \text{sinc}^2\left(\frac{\Delta k L}{2}\right) \quad (2)$$

where  $n$  is the refractive index of the material and  $L$  is the interaction length.

The central problem in parametric four-photon interactions is the conservation of momentum (phase matching), requiring  $\Delta k(\Delta \nu) = k_a + k_s - 2k_p = 0$ , where  $\Delta \nu$  is the frequency shift of Stokes and the anti-Stokes from the pump. For generating anti-Stokes wave in optical fibers, phase matching is achieved mainly by using either waveguide modes or fiber birefringence to compensate for the phase mismatch from the material dispersion

$\Delta k_m$ . Since  $\Delta k_m(\Delta\nu) > 0$  for fused silica in the UV range, negative phase mismatch from other sources is needed. Another important factor is the limitation introduced by a finite bandwidth laser source and fiber imperfections. The spread of the frequencies of the pump laser and fluctuations in  $k$  caused by the variations in fiber parameters lead to a finite coherence length. The fiber length should be shorter than the coherence length for maximum parametric anti-Stokes output.

## II. Phase matching using fiber modes

In an ordinary circular optical fiber,  $\Delta k$  (i.e. effective index) is determined by two factors, material dispersion and waveguide dispersion. We have

$$\begin{aligned}\Delta k &= k_s + k_a - k_{p1} - k_{p2} \\ &= 2\pi \left[ \frac{n_{\text{eff},s}(\lambda_s)}{\lambda_s} + \frac{n_{\text{eff},a}(\lambda_a)}{\lambda_a} - \frac{n_{\text{eff},p1}(\lambda_p)}{\lambda_p} - \frac{n_{\text{eff},p2}(\lambda_p)}{\lambda_p} \right]\end{aligned}\quad (3)$$

$$\text{with } \lambda_s = \lambda_p / (1 - \lambda_p \Delta\nu), \quad \lambda_a = \lambda_p / (1 + \lambda_p \Delta\nu)$$

$$\text{and } n_{\text{eff}} = n + b_{\Delta n},$$

where  $b = (n_{\text{eff}} - n_c) / \Delta n$  is the normalized propagation constant and  $\Delta n$  is the index difference  $n_c - n_{cl}$ , with  $n_c$  = core index,  $n_{cl}$  = cladding index. Therefore,

$$\begin{aligned}\Delta k &= 2\pi \left[ \frac{n(\lambda_s)}{\lambda_s} + \frac{n(\lambda_a)}{\lambda_a} - \frac{2n(\lambda_p)}{\lambda_p} \right] \\ &\quad + 2\pi \Delta n \left[ \frac{b_s(\lambda_s)}{\lambda_s} + \frac{b_a(\lambda_a)}{\lambda_a} - \frac{b_{p1}(\lambda_p)}{\lambda_p} - \frac{b_{p2}(\lambda_p)}{\lambda_p} \right]\end{aligned}\quad (4)$$

The first term is the material contribution  $\Delta k_m(\Delta\nu)$  and the second term is the waveguide contribution  $\Delta k_w(\Delta\nu)$ . Phase matching  $\Delta k_m(\Delta\nu) + \Delta k_w(\Delta\nu) = 0$  can be achieved by using various combinations of the fiber modes for the Stokes, anti-Stokes and pump.

The possibility of phase matching has already been described in the visible [2]. Fig. 1 shows a typical phase matching diagram for a pump wavelength of 500 nm [3]. The curve represents  $\Delta k_m(\Delta\nu)$  and the straight lines represent  $\Delta k_w(\Delta\nu)$  for different combinations of modes. The intersections correspond to the phase matching frequencies. It can be seen that different

combinations will result in different phase matched frequency shifts.

Phase matching from some particular mode combinations for pump wavelengths of 308 nm (XeCl), 249 nm (KrF) and 193 nm (ArF) were calculated with the assumptions of  $\Delta n = 0.02$ ,  $a = 2.5 \mu\text{m}$  (fiber core radius) using the approximate solution of the characteristic equation for the LP modes [4] and dispersion data of fused silica [5]. A few examples are shown in Table 1. The table also shows the coherence length as described in section IV. The results show that phase matching by using lower fiber modes should be achievable. At frequency shifts matching the vibrational energy levels (centered at  $\sim 460\text{cm}^{-1}$ ) of fused silica, phase matching is possible. To have efficient anti-Stokes output, we would like to use low-mode-number fibers, but they are not currently commercially available.

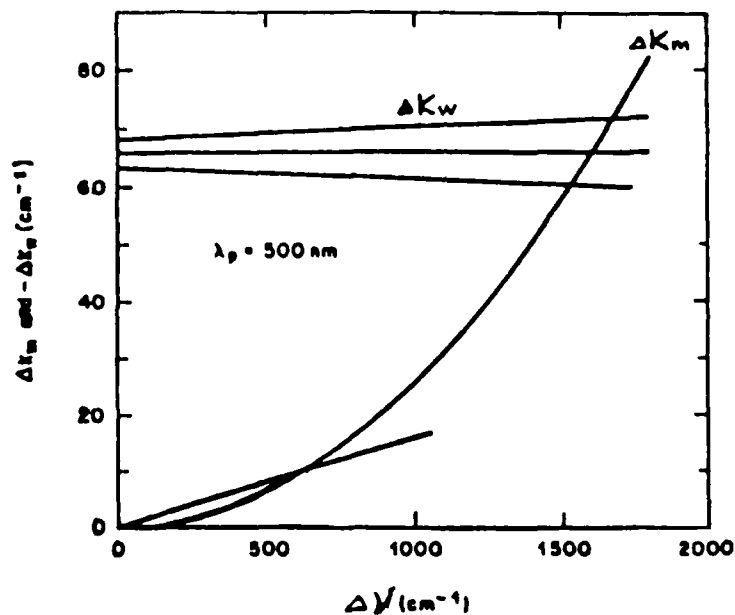


Fig. 1

Table 1. Calculated results for phase match with fiber modes

pump wavelength $\lambda_p (\mu\text{m})$	mode combination				phase matching freq shift ( $\text{cm}^{-1}$ )	coherence length (cm)
	$P_1$	$P_2$	A	S		
.308	02	01	11	01	170	106
.249	01	01	01	02	2415	50
.193	01	01	01	02	1495	13
.193	01	01	01	11	930	24
.193 ( $a=6.5\mu\text{m}$ )	11	01	01	02	458	42

### III. Phase matching using birefringent fibers

Some fibers have birefringence, defined as  $\delta n = n_x - n_y$ , with  $y$  and  $x$  denoting the slow and fast axis respectively. Phase mismatch  $\Delta k_{\text{B}}(\Delta\omega)$  is induced by this fiber birefringence. To achieve phase matching  $\Delta k_{\text{M}}(\Delta\omega) + \Delta k_{\text{B}}(\Delta\omega) = 0$ , the pump polarization should be aligned with the slow axis and Stokes as well as anti-Stokes polarization will be along the fast axis (since  $k_{\text{M}} + k_{\text{A}} > 2k_{\text{P}}$  from material dispersion). This gives

$$\Delta k_{\text{B}}(\Delta\omega) = 2\pi \left( \frac{n_x}{\lambda_s} + \frac{n_y}{\lambda_a} - \frac{2n_y}{\lambda_p} \right) = \frac{4\pi}{\lambda} \delta n \quad (5)$$

Fiber birefringence may be obtained from intrinsic built-in birefringence [6], bending-induced birefringence [7], stress-induced birefringence [8] or temperature-induced birefringence [9]. They all give a birefringence in the order of  $\delta n \approx 10^{-3}$ . Using the approximation for material phase mismatch  $\Delta k_{\text{M}}(\Delta\omega) = 2\pi \lambda^2 (d^2n/d\lambda^2)(\Delta\omega)/c$ , we have  $2\pi \lambda^2 (d^2n/d\lambda^2)(\Delta\omega)/c + (4\pi/\lambda)\delta n$  for phase matching  $\Delta k_{\text{M}}(\Delta\omega) + \Delta k_{\text{B}}(\Delta\omega) = 0$ .

Table 2 shows some calculated results for the frequencies which result in phase match, based on the same fiber parameters ( $\delta n = 0.02$  and  $a = 2.5 \mu\text{m}$ ) with different values of birefringence and useful wavelengths. The calculation is made under the assumption of single mode birefringent fibers so that material dispersion and birefringence are the only contributions to  $\Delta k$ . If using multimode fibers, the waveguide dispersion has to be considered, which leads to a much more complicated situation. The easy and efficient way to achieve stimulated four-photon mixing in birefringent fibers will depend on the availability of single mode uv fibers, which are not commercially available at this time. However, it is still worth using multimode birefringent fibers, especially employing bending-induced birefringence because of the convenience of varying the birefringence. Experimentally, we may achieve phase matching by tuning the birefringence through varying the bending radius [10].

Table 2. Calculated results for phase match with fiber birefringence

$\lambda_{\text{M}}$ ( $\mu\text{m}$ )	$\delta n$ ( $\times 10^{-3}$ )	$\Delta\omega$ ( $\text{cm}^{-1}$ )
.308	1.0	278
.308	5.0	622
.249	3.0	435
.249	9.0	754
.193	5.0	458
.193	9.0	609

#### IV. Coherence length

In stimulated four-photon parametric amplification, the gain bandwidth is determined by the curve of anti-Stokes intensity vs. frequency shift. If we use the peak power and the center frequency of the pump beam in the calculation of the phase matching condition and compute the anti-Stokes output intensity, we obtain the result of Eq. (2). However, the effective gain is reduced when the pump linewidth is larger than the parametric gain bandwidth. This is because frequencies other than the center frequency within the linewidth violate the previous phase matching condition. The effective gain has its maximum value only when the pump linewidth is much narrower than the gain bandwidth. A rule of thumb for the practical relationship between the gain bandwidth and the initial pump linewidth has been described by R. H. Stolen and J. E. Bjorkholm, which leads to a characteristic fiber length coherence length  $L_c$  [3]. The effective coherence length due to the finite linewidth of the pump is

$$L_c = \left[ \frac{2}{\lambda^2} \frac{d[\lambda D(\lambda)]}{d\lambda} (\Delta\omega_{pm}) (\delta\lambda_p)^2 \right]^{-1} \quad (6)$$

where  $\delta\omega_p$  is the initial pump linewidth,  $D(\lambda) = \lambda^2 (d^2 n_{eff}/d\lambda^2)$  is the dispersion and  $\Delta\omega_{pm}$  is the phase-matched frequency shift. The material dispersion is the dominating mechanism. When the fiber length is shorter than  $L_c$ , the pump linewidth is less than the gain bandwidth. The gain bandwidth of anti-Stokes decreases as the fiber length increases, which decreases the parametric (anti-Stokes) amplification. However, the Stokes gain bandwidth basically does not change with the fiber length and the Stokes intensity is proportional to  $L^2$ . Thus, long fibers favor the Raman Stokes amplification. Eq. (6) is a criterion of choosing the fiber length for achieving optimum anti-Stokes generation.

The calculated results of  $L_c$  are shown in Table 1 under the assumption of  $\delta\lambda_p = 4\lambda$ , the linewidth which the LUMONICS excimer lasers can achieve at 193 nm (ArF). For large frequency shift,  $L_c$  is small. This means that converting to short wavelength UV will be difficult. The problem is whether the coherence length is long enough that anti-Stokes would have enough gain to be observed. To improve the situation, we need to narrow the pump linewidth as much as possible.

In the derivation of the coherence length  $L_c$ , we take into account both  $\Delta k_m$  from material dispersion, and also dispersion from waveguide modes  $\Delta k_w$ . Even if we have ideal phase matching,  $\Delta k = \Delta k_m + \Delta k_w = 0$  for some mode combinations in perfect fibers, we will still have the phase mismatch  $\Delta k$  off center frequency. Without fluctuations and mode-mixing, transfer of power to anti-Stokes will build up only for one coherence length. However, fluctuations in  $k$  will occur due to the variations in fiber radius and index difference, and cause mode mixing. This mixing can cause the effective coherence length to be much larger than what we calculated from Eq. (6). A factor of hundreds in visible

stimulated four-photon mixing has been achieved [11]. Therefore, it appears that anti-Stokes may be generated and experience gain even for  $L \gg L_c$ . Because of the unavailability of low mode UV fibers we have been unable to pursue this approach.

#### V. Anti-Stokes wave generated from a Raman resonator

Because of the unavailability of low mode UV fibers, we consider the alternative of a Raman resonator. In the process of generating the anti-Stokes wave, the phase matching term in Eq. (1) is actually  $e^{i(\Delta\vec{k} \cdot \vec{r})}$ . Since in optical fibers,  $\vec{k}_s$ ,  $\vec{k}_p$  &  $\vec{k}_a$  are all along z axis, we could replace  $\Delta\vec{k} \cdot \vec{r}$  by  $\Delta k z$ . In bulk material, we may choose  $k_a$ ,  $k_s$  &  $k_p$  not necessarily in the same direction as z and we should use  $e^{i(\Delta\vec{k} \cdot \vec{r})}$ . If we can arrange  $\vec{k}_s$ ,  $\vec{k}_p$ ,  $\vec{k}_a$  in such way that  $\Delta\vec{k} = 0$ , then the phase matching condition will be satisfied. Fig. 2 shows a configuration for the wave vector match in generating anti-Stokes wave.  $R_1$  &  $R_2$  are mirrors which form a Raman resonator for a stable establishment of the Stokes wave.

An important point here is to generate the Stokes oscillation in the Raman resonator. The threshold condition for this is that the Raman gain is equal to the loss in the cavity. Assume an optical beam  $I_1$  starting at mirror  $R_1$ . After a round trip of travelling in the cavity, it becomes  $I_2$ . Then

$$I_2 = I_1 e^{gL_g} e^{-\alpha 2L} \quad (7)$$

where  $g$  is the gain,  $\alpha$  is the loss,  $L$  is the length of the resonator and  $L_g$  is the length with Raman gain  $g$ .

Considering loss due to material absorption and mirror transmission, we have

$$\alpha = \alpha_m - \frac{\ln(R_1 R_2)}{L} \quad (8)$$

where  $\alpha_m$  is the loss in the Raman medium,  $R_1$  &  $R_2$  is the reflectivity of mirror  $R_1$  &  $R_2$  respectively. Then

$$I_2 = I_1 e^{(gL_g - \alpha_m 2L + \ln R_1 R_2)} \quad (9)$$

For anti-Stokes generation, we need to arrange the beams (pump, Stokes and anti-Stokes) with angles which would satisfy  $\vec{k}_s + \vec{k}_a - 2\vec{k}_p = 0$ .

The candidates for materials working at 193 nm are quartz, water and acetonitrile. Here, we take quartz as an example to estimate whether it is possible to build an oscillation in such a resonator to generate the anti-Stokes wave.

For Raman scattering in quartz, the frequency shift  $\Delta\nu$  with

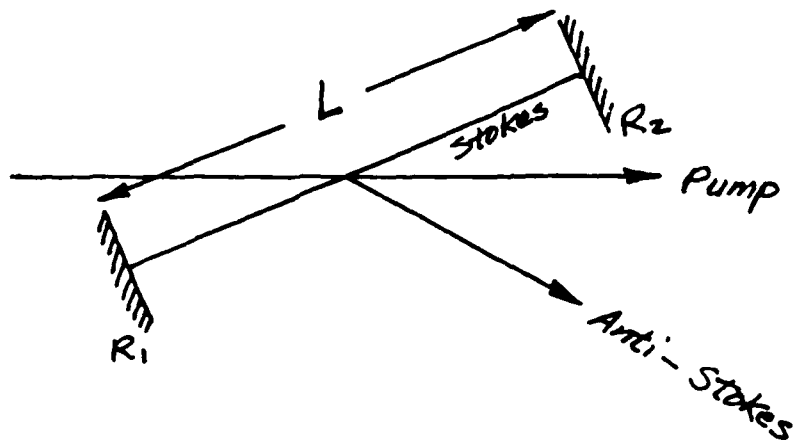


Fig. 2a Resonator

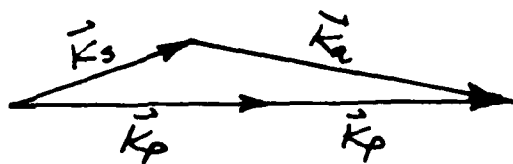


Fig. 2b Phase matching



max. gain is  $\sim 460 \text{ cm}^{-1}$ . At  $\lambda_p = 193 \text{ nm}$ ,

$$|k_p| = 5.077 \times 10^{11} \text{ cm}^{-1}$$

$$|k_s| = 5.132 \times 10^{11} \text{ cm}^{-1}$$

$$|k_a| = 5.023 \times 10^{11} \text{ cm}^{-1}$$

To achieve phase matching  $\vec{k}_s + \vec{k}_a - 2\vec{k}_p = 0$ , we need an angle of  $\sim 0.795^\circ$  between  $\vec{k}_p$  &  $\vec{k}_s$  and  $\sim 0.813^\circ$  between  $\vec{k}_p$  and  $\vec{k}_a$ .

The absorption coefficient  $\alpha_m$  for UV grade fused silica is  $0.05 \text{ cm}^{-1}$  [12], and the Raman gain coefficient for fused silica at  $193 \text{ nm}$  is  $\sim 2.8 \times 10^{-11} / I_p$  ( $\text{cm/Mw}$ ) [13]. Choose  $R = R_1 = R_2 = 0.95$  and  $L = 10 \text{ cm}$  for the resonator. Raman gain length  $L_g$  is determined by the focal size of the pump beam and the angle between the pump beam and the Stokes beam. Pump intensity is determined by the laser output energy and focal spot size. If we focus the beam to  $1 \text{ mm}$  diameter, we would have  $I_p \sim 100 \text{ Mw/cm}^2$  and  $L_g = 7 \text{ cm}$ . Substituting the above numbers into Eq. (9), we obtain

$$\alpha_m L + \ln(R_1 R_2)^{1/2} = -1 - 0.05 = -0.15$$

and the threshold intensity

$$I_{th} \sim 54 \text{ Mw/cm}^2$$

The numbers show that the threshold is not very high. The other two candidates, water and acetonitrile, should have a stronger Raman effect, but they also have higher absorption at  $193 \text{ nm}$ . On the other hand, if we focus the beam more, water and acetonitrile will be less likely to damage than quartz. Thus, at this point, we don't know which material will be more promising and plan to try both quartz and liquids.

## References

- [1] G. L. Eesley, Coherent Raman Spectroscopy. Pergamen Press 1981.
- [2] R. H. Stolen, "Phase-matched stimulated four-photon mixing in silica fiber waveguides," IEEE J. Quantum Electron. QE-11, 100, 1975.
- [3] D. Gloge, "Weakly guiding fibers," Appl. Opt. 10, 2252, 1971.
- [4] Roger H. Stolen and John E. Bjorkholm, "Parametric amplification and frequency conversion in optical fibers," IEEE J. of Quantum electron. QE-18, 1062, 1982.
- [5] American Institute of Physics Handbook. New York : Mcgraw-Hill, 1963, P6-25.
- [6] R.H. Stolen, M. A. Bosch, and C. Lin, "Phase matching in birefringent fibers," Opt. Lett. 6, 213, 1981.
- [7] Ken-Ichi Kitayama and Masaharu Ohashi, "Frequency turning for stimulated four-photon mixing by bending-induced birefringence in a single-mode fiber," Appl. Phys. Lett. 7, 619, 1982.
- [8] Masaharu Ohashi, Ken Ichi Kitayama, Yukinori Ishida, and Naoya Uchida, "Phase -matched light amplification by three-wave mixing process in birefringent fiber due to externally applied stress," Appl. Phys. Lett. 12, 1111, 1982.
- [9] Masaharu Ohashi, Ken-Ichi Kitayama, Nori Shibata and Shigeyuki Seikai, "Frequency turning of a Stokes wave for stimulated four-photon mixing by temperature induced birefringence change," Opt. Lett. 10, 77, 1985.
- [10] Nori Shibata, Masaharu Ohshi, Ken-Ichi Kitayma and Shigeyuki Seikai, "Evaluation of bending induced birefringence based on stimulated four-photon mixing," Opt. Lett. 10, 154, 1985.
- [11] R. H. Stolen, "Fiber Raman lasers," in Fiber and Integrated Optics, Ed. O. B. Ostrowsky. Plenum, 1979.
- [12] Optics Guide 3. Mells Griot, 1986.
- [13] A. Yariv, Quantum Electronics. John Wiley & Sons, Inc., 1979.



# UNIVERSITY OF SOUTHERN CALIFORNIA

## CENTER FOR LASER STUDIES

Denney Research Building

Elsa Garmire, Director

Los Angeles, CA 90089-1112

Susan D. Allen, Associate Director

(213) 743-6418

July 25, 1987

Dr. Howard Schlossberg  
AFOSR  
Bolling AFB  
Washington DC

Dear Howie:

Enclosed is our final report on the two-year program which you funded. This work led to one MS thesis, three publications and three public presentations. We believe that this represents excellent results for the small level of funding. You will find the technical results on color center formation in UV fibers particularly interesting.

We are now hoping that we can obtain some funding from your nonlinear optics program. This is urgent because several of our small and short programs, including yours, have recently ended and it is imperative that the students can receive additional support.

There are several possible projects which we want to carry out. These are briefly outlined here, in order of our interest. Please let us know which interest AFOSR. We need the program to begin in this fiscal year, since otherwise at least one student will have to be laid off.

### 1. NONLINEAR OPTICAL PROPERTIES OF WIDE BAND SEMICONDUCTORS

We propose to study the nonlinear optical properties (both saturable absorption and nonlinear refractive index) at the bandgap of ZnSe/ZnSSe multiple quantum wells and single-crystal GaN as well as polycrystalline  $\text{In}_2\text{O}_3$ ,  $\text{CdSnO}_4$  and  $\text{CdIn}_2\text{O}_4$ . The study will follow the general outline of our previous work in GaAs and GaAs/GaAlAs multiple quantum wells which have shown extremely large nonlinearities. This means that measurements will be made of both saturable absorption and the nonlinear index through the use of nonlinear etalons. However, we will now be looking, for the first time, at wide direct bandgap materials.

This idea has developed out of our current UV research on the program which you funded and our ability to use stimulated Raman effect to "tune" the wavelength of the excimer laser. Single crystal materials will be provided by scientists at NTT (an

outgrowth of my trip to Japan last summer). They have provided us with samples of both GaN and ZnSe, in thin film and in waveguide configurations, and have promised whatever we need. Samples of sputtered indium tin oxide and related compounds are being provided by Kate Zachremska, a visitor from Poland who studied CdIn<sub>2</sub>O<sub>4</sub> for her PhD thesis.

In a preliminary experiment on single crystal ZnSe waveguides we observed absorption-induced optical bistability. While this is not as interesting as electronic nonlinearities, it demonstrates our ability to obtain these materials and to perform experiments with them. Galley proofs of this work are enclosed.

We request that AFOSR fund a research project to understand the electronic nonlinearities at the bandgap of such ZnSe samples, both as bulk and as strained-layer superlattices. The scientists at NTT have promised to provide us with a continuing source of material, including multiple quantum wells, but we require funding to perform the experiments. The flash-lamp-pumped dye laser which you provided to the Center through Rothschild as PI will be an ideal tunable source for these studies. Both etalons and waveguides will be studied.

The scientific interest in ZnSe is the large energy separation of the exciton from the bandedge (much larger than in GaAs) and the expectation that the nonlinearities should be especially large. Comparison of bulk ZnSe and multiple quantum wells should yield similar information to that which has recently been obtained in GaAs MQW's. NTT can also provide us with mixed crystals of ZnSSe, allowing us to tune the bandgap over some range.

A related study in ZnSe will be the measurement of electro-absorption. This effect, observed in III-V's, has led to enhanced modulation near the bandgap and we expect similar results in the II-VI's.

A second major study will be the measurement of optical nonlinearities in UV and near-UV direct-gap materials. The first investigations will be on single crystal GaN. Researchers at NTT have provided this material. We have tried preliminary experiments and found that our excimer laser does not match the bandgap. However, stimulated Raman scattering, as studied in our past grant from you, will provide a tunable source at exactly the required wavelengths. This will be the first measurement of optical nonlinearities in UV semiconductors.

The same experimental apparatus will be used to study the sputtered thin films of transparent conductors, such as ITO, as well as indium oxide, cadmium tin oxide, and cadmium indium oxide. Nonlinear effects have never been investigated in this important class of transparent contacts.

This wide bandgap study is our first proposal. The program outlined here can be completed by two graduate students, with some fraction of my time and some assistance from Kachrewska; it should cost on the order of \$150,000 a year for three years. We already have the lasers and only some diagnostic equipment is required to support the efforts. The results would give the first information on the nonlinear properties of wide bandgap semiconductors.

## 2. TWO-WAVE AND FOUR-WAVE MIXING IN SEMICONDUCTORS

We propose a basic study of photorefractive effects in GaAs, InP and ZnSe in order to achieve the largest possible two-wave and four-wave mixing. This is an outgrowth of a project we recently completed in two-wave mixing and which is included in preprint form. We showed in this paper that it is possible to use the polarization properties of the zincblende structure to remove the unwanted background.

In order for the photorefractive effect in semiconductors to become important as a nonlinear mechanism, it is necessary to achieve two-wave gain larger than the inherent loss in the medium. The result of a recent analysis is that this can be accomplished by applying a moving grating to undoped, semi-insulating samples. Operating near the bandgap will further enhance the photorefractive effect. We propose to study and compare GaAs, InP, semi-insulating GaInAsP grown in our laboratory, and ZnSe provided by NTT.

The importance of this research is the fact that photorefractivity is an energy-dependent effect which can be ultra-fast, if excited by pulses, or ultra-slow if excited by weak cw light. The effect can be switched on or off depending on the optical configuration. Thus it makes a really controllable nonlinearity. The ability to use semiconductors will have tremendous implications for practical devices. The range of materials which are available to us and our new method of making measurements makes our research unique.

The level of effort will be one student plus a small fraction of another to provide materials plus some of my time. A level of about \$75,000 per year should be sufficient, plus enough capital equipment money to buy a diode-pumped YAG laser.

## 3. NONLINEAR EFFECTS IN GaAlAsP materials

We propose to grow our own thin films of GaInAsP by liquid phase epitaxy and to measure the nonlinear properties of these films over a wavelength range from 1.06 to 1.55  $\mu\text{m}$ .

We have already demonstrated an ability to grow high quality GaInAsP with a bandgap variable anywhere from 1.3  $\mu\text{m}$  to 1.06  $\mu\text{m}$ . This is the same apparatus we previously used to grow semi-conductor lasers. I visited a laboratory in the Soviet Union which has demonstrated high quality multiple quantum wells from similar apparatus. We propose to grow such films in this program. We have already recently demonstrated the ability to grow films with a bandgap at 1.06  $\mu\text{m}$  and we have made preliminary measurements of nonlinear optical properties in Schottky barriers, which will be reported at OSA.

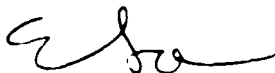
The use of GaInAsP has two main advantages. First, the substrate is transparent so that nonlinear effects can be measured directly without removing the substrate, as required for GaAs. Secondly, the ease of growth means that multiple quantum wells and waveguide configurations can both be grown and compared to bulk films. The liquid phase epitaxial technique allows considerable flexibility for making samples which can be measured easily.

We have available 1.06 and 1.33  $\mu\text{m}$  Nd:YAG lasers. A color center laser will provide the source at 1.55  $\mu\text{m}$ . We will use the same experimental techniques we have used in measurements of GaAs.

The required level of effort is two students - one for the sample preparation and the other for the measurements. This should be at the rate of approximately \$120,000 per year.

I certainly hope that one of these programs will be of interest to the Air Force. May we look forward to your suggestions? We can prepare a formal proposal in a matter of days, as each program is already completely thought out.

Best Regards,



Elsa Garmire

## Optical bistability and nonlinear switching due to increasing absorption in single-crystal ZnSe waveguides

B. G. Kim and E. Garmire

*Center for Laser Studies, University of Southern California, Los Angeles, California 90089-1112*

N. Shibata and S. Zembutsu

*Ibaraki Electrical Communication Laboratories, Nippon Telegraph and Telephone Corporation, Tokai, Ibaraki 319-11, Japan*

(Received 6 March 1987; accepted for publication 18 June 1987)

Optical nonlinear switching and bistability due to increasing absorption have been observed in single-crystal ZnSe waveguides with contrast ratios of 16/1 and switching times of 10  $\mu$ s at 15 mW of argon laser light. Switching energy is improved over the bulk by a factor of 200.

The dream of a low-threshold all-optical switching has led to the recent exploration of a variety of guided-wave nonlinear devices, from nonlinear guided waves<sup>1</sup> and prism couplers<sup>2</sup> through directional couplers<sup>3</sup> to Fabry-Perot resonators within guided waves.<sup>4</sup> At the same time several researchers have reported bistability due to increasing absorption in a variety of materials such as amorphous GeSe,<sup>5</sup> ZnSe,<sup>6</sup> CdS,<sup>7</sup> GaAs/GaAlAs multiple-quantum wells,<sup>8</sup> and InSb.<sup>9</sup> We report here for the first time optical bistability and nonlinear optical switching due to increasing absorption in a ZnSe single-crystal waveguide. This waveguide configuration decreases the energy threshold by more than a factor of 200 over bulk results,<sup>6</sup> and we predict optimized threshold switching power of less than a milliwatt. The advantage of absorption-induced bistability is that it does not require a Fabry-Perot resonator or phase-matching element; this means that single-mode guides and careful control of the input wavelengths are not required, unlike most other nonlinear guided switches. The switching times of 10  $\mu$ s that were obtained are short enough to be useful for some applications, and predictions are that submicrosecond operation is possible.

The waveguides were single-crystal ZnSe films grown by metalorganic vapor phase epitaxy (MOVPE) on GaAs substrates. The structures produced were either 8- $\mu$ m-thick multimode waveguides grown on 2- $\mu$ m ZnS<sub>0.98</sub>Se<sub>0.02</sub> cladding layers, or 2- $\mu$ m-thick antiwaveguides grown directly on the GaAs substrate. The refractive index of the ZnSe waveguide layer is 2.72 and that of the cladding is 2.70 at  $\lambda = 0.5$   $\mu$ m. The cladding provides a guiding dielectric discontinuity to confine the beam in the guiding layer. Planar waveguide samples of length 530 and 830  $\mu$ m were used to investigate bistability and nonlinear switching and were compared to an antiwaveguide sample of length 560  $\mu$ m. The samples were mounted on a thin aluminum stud which was thermally isolated from the holder.

Studies of optical switching were made using the 0.488- $\mu$ m line of the Ar<sup>+</sup> laser focused by a 40 $\times$  microscope objective into the waveguide layer. The light polarization and guide geometry were such as to excite the TE mode in the slab waveguide. We have used two different methods to modulate the input to the waveguide. First, we used the first-order diffracted beam from an acousto-optic modulator to control the peak power of the incident beam, and a chopper was used to create a time evolution of the input to the waveguide. Second, we directly used the modulated first-order diffracted beam from an acousto-optic modulator. The duty cycle of the input in both cases was around 1% to ensure that there was no overall heating of the sample. We did not see any major differences in the output characteristics obtained from the two different modulation methods. Duty cycles of up to 4% did not change the switching characteristics. The transmitted beam from the waveguide was imaged onto a photodetector using a 20 $\times$  microscope objective. The incident and transmitted powers were monitored using conventional Si photodiodes. A typical time trace of the incident and transmitted beam intensity is shown in Fig. 1. The threshold switching power into the waveguide, after correcting for reflection and coupling losses, was 15 mW. This is considerably smaller than previously measured threshold powers in bulk polycrystalline ZnSe.<sup>6</sup> As with all absorption-induced bistability, increasing intensity causes the

transmission to switch from the high state to the low state. Our measured on-switching times were around  $10\mu\text{s}$ . At the end of the pulse the device switches back to the high transmission state in the thermal lifetime, measured here to be  $20\mu\text{s}$ . This is 20 times faster than previously measured switching times in the bulk of polycrystalline ZnSe.<sup>6</sup> A typical absorption-induced bistability transfer curve obtained from the ZnSe waveguide is shown in Fig. 2.

According to our data the threshold switching power did not depend on the sample length, as expected for absorption-induced bistability in the steady-state regime. What does depend on length is the contrast ratio. We observed on-off contrast ratios as large as 16/1 in the sample of length  $830\mu\text{m}$ , while contrast ratios as large as 6/1 were observed in the sample with length  $530\mu\text{m}$ . These contrasts were measured roughly  $100\mu\text{s}$  after switching, long enough time to achieve temperature uniformity in the direction of propagation. It is thus possible to assume that the absorption coefficient of the ZnSe waveguide before switching is  $\alpha_1$  and after switching is  $\alpha_2$ , the contrast ratio is given by

$$\frac{\exp(-\alpha_1 L)}{\exp(-\alpha_2 L)} = \exp[(\alpha_2 - \alpha_1)L]. \quad (1)$$

For the sample with the length of  $530\mu\text{m}$ , a contrast ratio of 6/1 was measured. From this we can calculate

$$\alpha_2 - \alpha_1 = 33.8\text{ cm}^{-1} \quad (2)$$

and predict the contrast ratio of a sample of length  $830\mu\text{m}$  as 16.5. This value agrees very well with the observed value 16/1.

To determine the attenuation constant of the propagating modes in the ZnSe waveguide, we compared the input-output ratio of the guided-mode power for the two lengths under low input power. We determined the low-power absorption coefficient of our waveguide sample to be  $7.5\text{ cm}^{-1}$ . This data is consistent with the published data for bulk polycrystalline material.<sup>6</sup> We measured the transmittance of the focusing microscope objective lens used in the experiment as 84% and calculated the reflectance at the interface between air and the ZnSe surface as 21%. We calculated the coupling efficiency from the focused Gaussian beam into the waveguide as 79%. Assuming these values we calculate a threshold switching power of as little as 15 mW into the guide.

We observed similar optical switching and bistability from the antiwaveguide sample. This means that the switching from high transmission state to low transmission state observed in the ZnSe waveguide does not occur from driving a waveguide nonlinearly through cutoff. Thus, we could conclude that the observed optical bistability in the ZnSe waveguide comes from the absorption-induced mechanism. One advantage of the geometry reported here is that only a single nonlinear mechanism was observed. This single-mechanism switching can be differentiated from those which involve nonlinear couplers<sup>2</sup> or resonant cavity waveguides.<sup>4</sup> The existence of only a single nonlinear mechanism provides the most useful devices for system applications and for basic studies.

Since the cover of waveguide is air, we can neglect heat transfer to the air. This means that the local temperature rise in the waveguide is almost twice as high as that of bulk at the same optical power density. Thus, the threshold switching power in this waveguide will be twice as low as that of bulk even without considering diffraction effects. Although the threshold is apparently not length dependent, the waveguide geometry allows considerable improvement in contrast ratio at low input power levels by allowing use of relatively long sample lengths without diffraction.

The other important advantage of the use of waveguides is that by confining the light to a small spot, dramatic improvements in response time are possible. Use of strip-loaded channel waveguides will allow further improvements in response time. A lower limit to the switch-off time can be calculated from the thermal conduction time assuming a  $8\mu\text{m} \times 8\mu\text{m}$  channel.<sup>10</sup>

$$T = \frac{r^2 C_p \rho}{4K} = 0.4\mu\text{s}, \quad (3)$$

where  $\rho = 5.27\text{ g/cm}^3$ ,  $C_p = 0.35\text{ J/g}^\circ\text{C}$ ,  $K = 0.18\text{ W/cm}^\circ\text{C}$ , and  $r = 4\mu\text{m}$ . Of course transient nonuniformities in temperature over the length of the waveguide may affect the contrast ratio. Further work is under way to investigate this.

Comparable nonlinear switches can be expected at 0.83 and  $1.3\mu\text{m}$  wavelengths when suitable GaAlAs or GaInAsP materials are chosen and étalon effects<sup>1</sup> are eliminated. We believe that these devices may play a useful role in future integrated and fiber optical systems, even though the thermal effects are on the order of a microsecond. The ability to use cavityless multimode or single-mode waveguide geometries, along with thresholds on the order of 1 mW and no requirement on careful wavelength tuning of laser, input coupler, or integrated optics interferometer, means that these nonlinear devices can be compatible with inexpensive semiconductor lasers.

This work was supported in part by the Office of Naval Research and in part by the National Science Foundation.

<sup>1</sup>H. Vach, C. T. Seaton, G. I. Stegeman, and I. C. Khoo, *Opt. Lett.* **9**, 238 (1984).

<sup>2</sup>G. Assanto, B. Svensson, D. Kuchibhatla, U. J. Gibson, C. T. Seaton, and G. I. Stegeman, *Opt. Lett.* **11**, 644 (1986).

<sup>3</sup>S. M. Jensen, *IEEE J. Quantum Electron.* **QE-18**, 1580 (1982).

<sup>4</sup>A. C. Walker, J. S. Aitchison, S. Ritchie, and P. M. Rodgers, *Electron. Lett.* **22**, 366 (1986).

<sup>5</sup>J. Hajto and I. Janossy, *Philos. Mag.* **B 47**, 347 (1983).

<sup>6</sup>M. R. Taghizadeh, I. Janossy, and S. D. Smith, *Appl. Phys. Lett.* **46**, 331 (1985); A. K. Kar and B. S. Wherrett, *J. Opt. Soc. Am.* **B 3**, 345 (1986).

<sup>7</sup>K. Bohnert, H. Kalt, and C. Klingshirn, *Appl. Phys. Lett.* **43**, 1088 (1983); H. Rossmann, F. Henneberger, and J. Voigt, *Phys. Status Solidi B* **115**, K63 (1983); M. Dagenais and W. F. Sharfin, *Appl. Phys. Lett.* **45**, 210 (1984).

<sup>8</sup>D. A. B. Miller, A. C. Gossard, and W. Wiegmann, *Opt. Lett.* **9**, 162 (1984).

<sup>9</sup>B. S. Wherrett, F. A. P. Tooley, and S. D. Smith, *Opt. Commun.* **52**, 301 (1984).

<sup>10</sup>H. S. Carslaw and J. C. Jaeger, *Conduction of Heat in Solids* (Clarendon, Oxford, 1959), pp. 255-281.



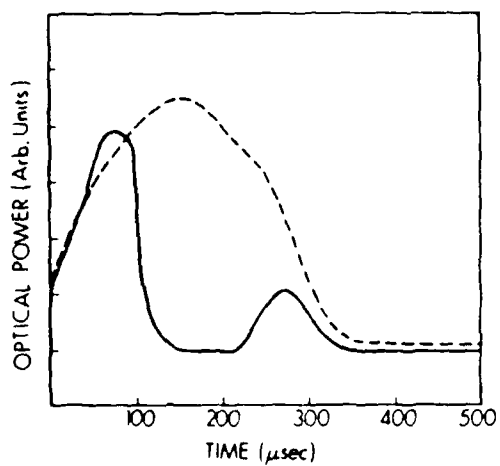


FIG. 1. Absorption-induced optical switching in a ZnSe waveguide. Dashed line is the input pulse from modulated  $\text{Ar}^+$  laser. Solid line is the output of the waveguide as a function of time. The amplitude scale of input and output pulses are independent. Vertical scale is arbitrary.

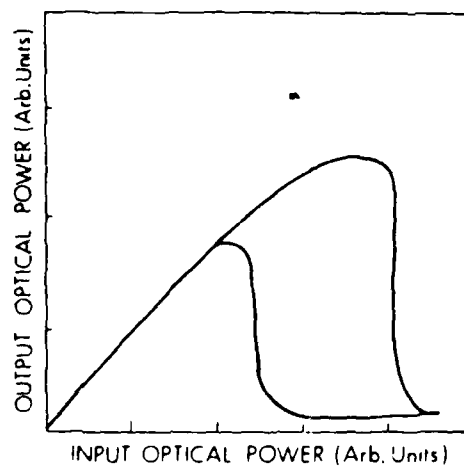


FIG. 2. Light output as a function of input, demonstrating the typical absorption-induced bistability transfer curve obtained from a ZnSe waveguide.

## Enhanced beam coupling modulation using the polarization properties of photorefractive GaAs

Afshin Partovi

Center for Laser Studies, University of Southern California, Los Angeles, California 90089-1112, and Jet Propulsion Laboratory, California Institute of Technology, Pasadena, California 91109

Elsa M. Garmire

Center for Laser Studies, University of Southern California, Los Angeles, California 90089-1112

Li-Jen Cheng

Jet Propulsion Laboratory, California Institute of Technology, Pasadena, California 91109

(Received 23 March 1987; accepted for publication 2 June 1987)

We report observation of a rotation in the polarization of the two photorefractive recording beams in GaAs for a configuration with the internally generated space-charge field along the (110) crystallographic orientation. This rotation is a result of simultaneous constructive and destructive beam coupling in each beam for the optical electric field components along the two electro-optically induced principal dielectric axes of the crystal. By turning one of the beams on and off, the intensity of the other beam after the crystal and a polarization analyzer can be modulated by as much as 500%. This result is of particular importance for optical information processing applications.

In the past few years, the photorefractive effect has been demonstrated in various semi-insulating semiconductors such as undoped GaAs,<sup>1</sup> GaAs:Cr, InP:Fe,<sup>2</sup> and CdTe.<sup>3</sup> Recently, GaAs has been shown to possess picosecond response times in the near infrared resulting from its large carrier mobilities.<sup>4</sup> Although these semiconductors are very sensitive, their electro-optic coefficients are relatively small. Therefore, large two-beam coupling coefficients and hence sizeable energy transfers between the two beams have not been feasible in these materials. In a 5-mm-thick GaAs crystal, 10–20% change in beam intensity is typically possible by photorefractive energy transfer.<sup>1,5</sup> Larger intensity modulations (up to 50%) have been observed by application of an external electric field to the sample.<sup>6</sup> By utilizing the polarization properties of photorefractive recording in Bi<sub>12</sub>SiO<sub>20</sub> (BSO), Herriau *et al.*<sup>7</sup> have demonstrated an increase in the contrast of images created by photorefractive two-wave mixing. In this letter we describe the polarization properties of beam coupling in  $\bar{4}3m$  crystals such as GaAs. It is found that under certain conditions the photorefractive effect may result in a rotation of the polarization of the two recording beams. This makes it possible to use an analyzer to suppress the large unwanted dc portion of the signal beam. Consequently, for the first time, large modulation (> 500%) of beam intensities can be obtained in photorefractive semiconductors.

Figure 1 illustrates the essential features of the experimental condition. A signal beam of intensity  $I_s$  and a reference beam of intensity  $I_R$ , polarized along the (001) crystal orientation intersect in the crystal with an interference vector  $K_G$  along the (110) crystallographic axis. The internally generated space-charge electric field is also along this direc-

tion. Figure 2 shows the resulting principal dielectric axes in the material through the  $r_{41}$  electro-optic tensor element for such a space-charge field. The electric field vector of the incident beams can be decomposed into equal components along these two axes. The refractive index change in the material for the two components,  $E_x$  and  $E_y$ , is given by  $\Delta n_{x,y} = \pm 1/2 n_b^3 r_{41} E_{sc}$ , where  $n_b$  is the background refractive index of the material,  $r_{41}$  is the effective electro-optic coefficient, and  $E_{sc}$  is the internally generated space-charge field. These two components experience two different gratings with equal modulation depth and 180° spatial phase difference. In the absence of an externally applied electric field, these photorefractive index gratings are 90° out of phase with the interference pattern. Since the relative position of the index grating with respect to the interference pattern determines the direction of beam coupling, the two polarization components couple optical energy in opposite directions. Signal beam amplification in two-beam coupling is commonly defined as the ratio  $I_s$  (with reference beam present)/ $I_s$  (without reference beam present). For the two polarizations, this ratio, the effective gain, is given by<sup>8</sup>

$$\gamma_{\pm} = \frac{(1 + \beta) \exp(\Gamma_{\pm} d)}{1 + \beta \exp(\Gamma_{\pm} d)}, \quad (1)$$

where  $\beta = I_s / I_R$  is the ratio of the intensities of the incoming beams and  $d$  is the thickness of the crystal. The coupling coefficient for the two polarizations can be written as<sup>9</sup>  $\Gamma_{\pm} = \pm n_b^3 r_{41} \delta$ , where  $\delta$  depends on various fundamental material properties and experimental conditions such as the angle between the two beams. In traveling through the crystal, one of the components of the electric field vector of the

\*P. Gunter, Phys. Rep. 93, 199 (1982).

<sup>9</sup>N. V. Kukhtarev, V. B. Markov, S. G. Odulov, M. S. Soskin, and V. L. Vinetski, Ferroelectrics 22, 961 (1979).

<sup>10</sup>A. M. Glass, M. B. Klein, and G. C. Valley, Electron. Lett. 21, 220 (1985).

<sup>11</sup>Y. Shi, D. Psaltis, A. Marrakchi, and A. R. Tanguay, Jr., Appl. Opt. 22, 3665 (1983).

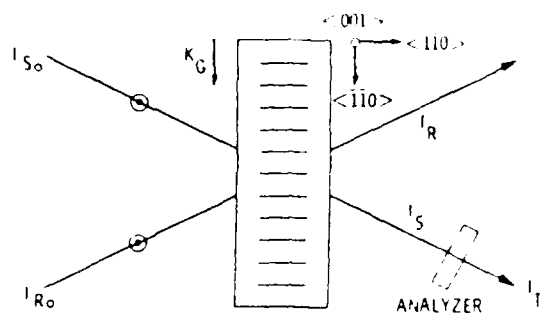


FIG. 1 Schematic diagram of the experimental arrangement for two-beam coupling

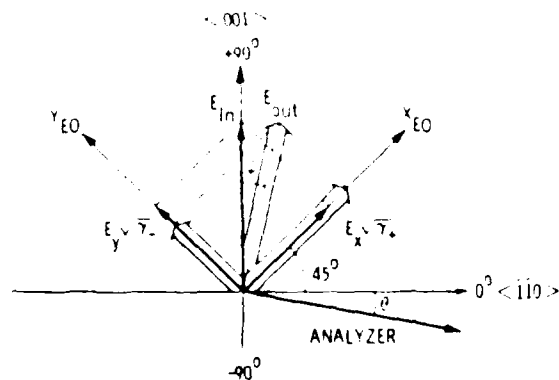


FIG. 2 Rotation of the signal beam polarization due to the photorefractive effect in 43m crystals. The crystal orientation and polarization of the incoming beam are shown.  $X_m$  and  $Y_m$  are the electro-optically induced principal dielectric axes of the material. The analyzer angle  $\theta$  is defined in terms of the angles shown on the axes.

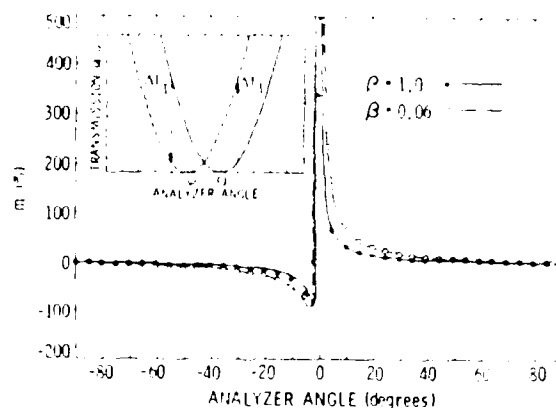


FIG. 3 Calculated and measured percent modulation  $m$  as a function of the analyzer angle for two different beam intensity ratios  $\beta$ . The total incident intensity is  $30 \text{ mW/cm}^2$  in both cases. The curves are plots of Eq. (4) with the rotation angle  $\psi$  calculated from Eqs. (1) and (3) using the value of  $I_{R0} = 0.2 \text{ cm}^{-1}$  measured for the  $K_G \parallel (001) \parallel$  configuration and the respective values of  $\beta$ . The inset shows the transmission of the analyzer with (dashed line) and without (solid line) the reference beam present for an arbitrary angle of rotation  $\psi$  near the transmission minimum point.

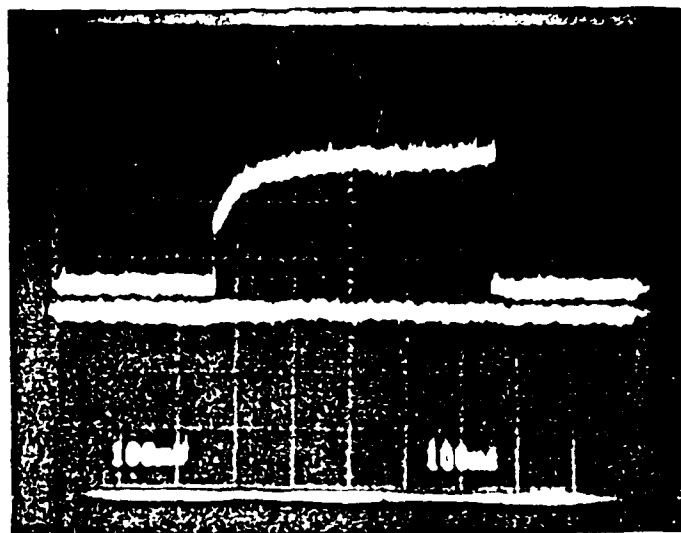


FIG. 4 Oscilloscope trace of transmitted beam intensity modulation for the  $K_G \parallel (110) \parallel$  orientation with  $\beta = 0.06$ . The analyzer angle was  $+2^\circ$ . The lower trace is obtained by blocking both of the beams.

amplification) while the other component suffers loss. Figure 2 shows the two electric field components of the signal beam into and out of the crystal. Due to the increase of one of the components, and the decrease in the other, the electric field vectors of the two writing beams are slightly rotated. The rotation of the polarization for the two beams is in opposite directions.

The inset in Fig. 3 shows the intensity of the signal beam transmitted through the crystal and an analyzer as a function of the analyzer angle near the transmission minimum point with and without the reference beam, where  $\psi$  is the angle of rotation due to the presence of the reference beam. The transmitted intensity  $I_T$  can be written as

$$I_T = I_s \exp(-\alpha d) \sin^2(\theta + \psi), \quad (2)$$

where  $\theta$  is as described in Fig. 2 and  $\alpha$  is the absorption coefficient of the crystal. The angle  $\phi$  is defined as zero without the reference beam present, and in the presence of the reference beam,  $\phi$  is equal to  $\psi$ , the angle of photorefractive rotation described above.

The two electric field components of the signal beam after the sample are  $E_x$  (with  $I_{R_0}$ ) =  $\sqrt{\gamma_+}$   $E_x$  (without  $I_{R_0}$ ), and  $E_y$  (with  $I_{R_0}$ ) =  $\sqrt{\gamma_-}$   $E_y$  (without  $I_{R_0}$ ). From Fig. 2 it can be seen that the rotation angle

$$\psi = 45^\circ - \tan^{-1}(\sqrt{\gamma_-/\gamma_+}). \quad (3)$$

The arrows in the inset in Fig. 3 show the change in transmitted intensity  $I_T$  with and without the reference beam for two arbitrary analyzer angles. We define the modulation of the transmitted beam,  $m = \Delta I_T / I_T$  (when the reference beam is not present). Using Eq. (2) this ratio is given by

$$m = [\sin^2(\theta + \psi) - \sin^2(\theta)] / \sin^2(\theta). \quad (4)$$

Note that this relation is independent of the absorption coefficient of the material.

The material used in this experiment was a 5.3-mm-thick semi-insulating liquid encapsulated Czochralski (LEC) grown, undoped GaAs sample. The photoconductive trap sites in undoped GaAs are believed to be stoichiometry-related EL2 centers.<sup>1,10</sup> In this experiment no external field was applied to the crystal. The output beam from a 1.7-mW HeNe laser operating at 1.15  $\mu\text{m}$  was split into two beams such that the bisector of the angle between them (86° outside the crystal) was perpendicular to the crystal surface as shown in Fig. 1. The resulting grating period of 0.84  $\mu\text{m}$  is near the optimum value for beam coupling in this sample. The total incident intensity on the crystal was 30 mW/cm<sup>2</sup>. The value of the coupling coefficient,  $\Gamma_+$ , was measured experimentally to be equal to 0.2 cm<sup>-1</sup> for the  $K_G \parallel (001)$  case in the same crystal without an analyzer, under otherwise equal experimental conditions. This orientation which is normally used in beam coupling experiments utilizes only one principal dielectric axis and therefore produces a measurable value for  $|\Gamma_+|$ . Applying this value to Eqs. (1) and (3), the rotation angle for the  $K_G \parallel (110) \parallel (110)^\circ$  orientation was calculated for two beam ratios. For  $\beta = 1$ , the rotation angle  $\psi = 1.53^\circ$ , while for  $\beta = 0.06$ , the angle increases to  $\psi = 3.03^\circ$ . Plots of Eq. (4) using these values of  $\psi$  are shown in Fig. 3. Figure 3 also shows the experimental data of  $m$  as a function of the analyzer angle (defined in Fig. 2) for the two

beam ratios in the  $K_G \parallel (110)$  configuration. In this figure, zero degree corresponds to an analyzer position along the (110) crystal axis and is therefore a point of minimum transmission. Without the analyzer no energy transfer from one beam to another was detected. In both cases the theoretical fit to the experimental data is very good.

Figure 4 shows an oscilloscope trace of the output of the signal beam detector. The lower trace is obtained by blocking both of the beams before the crystal and represents the background level. The upper trace shows the result of unblocking the signal and then both of the beams. In the presence of the reference beam, the transmitted intensity  $I_T$  rises with a characteristic built-up time of the photorefractive effect to a maximum value. Upon blocking the reference beam, this intensity drops to its original value. The experimental modulation of 500% was limited by the finite extinction ratio of the analyzer.

Suppression of the dc background in the system described above offers promise for image processing and other information processing applications requiring large contrast ratios. The higher contrast ratio is, however, achieved at the price of a drop in overall transmission. Taking absorption of the crystal into account, the on-state transmitted intensity shown in Fig. 4 was 0.45% of  $I_{s_0}$ . "ON"

The analysis described above is valid for all photorefractive materials with electro-optic tensor matrices similar to GaAs (43m crystallographic symmetry). Materials with 23 crystal symmetry such as BSO have similar matrix elements. Incoherent to coherent conversion of images via four-wave mixing in BSO has been demonstrated by Shi *et al.*<sup>11</sup> Comparable results using the polarization rotation properties in two-wave mixing can be achieved in GaAs. Two wave mixing provides a more flexible and simpler method of implementing this device than four-wave mixing. Furthermore, since both positive and negative intensity modulations are possible by rotation of the analyzer, positive and negative images are available with this device. The rotation of the polarization can be further enhanced by increasing the coupling coefficient, such as by application of an external field or using moving grating techniques.

The work described in this letter was carried out jointly at the University of Southern California and the Jet Propulsion Laboratory, California Institute of Technology. The work at the Jet Propulsion Laboratory under agreements with the National Aeronautics and Space Administration, was supported by Caltech President's Fund and the Defense Advanced Research Projects Agency. The work at the Center for Laser Studies was partially supported by the National Science Foundation and the Army Research Office.

<sup>1</sup>M. B. Klein, Opt. Lett. 9, 350 (1984).

<sup>2</sup>A. M. Glass, A. M. Johnson, D. H. Olson, W. Simpson, and A. A. Ballman, Appl. Phys. Lett. 44, 948 (1984).

<sup>3</sup>J. Strait and A. M. Glass, J. Opt. Soc. Am. B 3, 342 (1986).

<sup>4</sup>G. C. Valley, A. L. Smith, M. B. Klein, K. Bohnert, and I. F. Bogges, Opt. Lett. 11, 647 (1986).

<sup>5</sup>L. J. Cheng and A. Partovi, Appl. Phys. Lett. 49, 1456 (1986).

<sup>6</sup>G. Albanese, J. Kumar, and W. H. Steier, Opt. Lett. 11, 650 (1986).

<sup>7</sup>J. P. Hérnau, J. P. Huignard, A. G. Apostolidis, and S. Mallick, Opt. Commun. 56, 141 (1985).

